Excitation of Silicon and Diamond Microsphere Whispering Gallery Modes by Femtosecond Laser Written Glass and Diamond Waveguides, and a Glass Fiber Coupler

by

Hüseyin Ozan Çirkinoğlu

A Thesis Submitted to the
Graduate School of Sciences and Engineering
in Partial Fulfillment of the Requirements for
the Degree of

Master of Science

in

Optoelectronics and Photonics Engineering

Koç University

August 2017

Koç University

Graduate School of Sciences and Engineering

This is to certify that, I have examined this copy of a master's thesis by

Hüseyin Ozan Çirkinoğlu

and have found that, it is complete and satisfactory in all respects,
and that, any and all revisions required by the final
examining committee have been made.

Committee Members:

____

Ali Serpengüzel, Ph.D. (Advisor)

____

Alper Kiraz, Ph.D.

____

Onur Ferhanoğlu, Ph.D.

Date: ______________________________

ABSTRACT

Whispering gallery modes (WGMs) are the optical resonances, where light is trapped inside a dielectric and symmetric cavity by total internal reflection (TIR) on the boundary facets. Due to the unique optical properties, such as very high quality factors, and very narrow linewidths, due to the long photon lifetime inside the cavity, and confinement of the field in very small mode volumes, resulting in high power densities, cavities of different geometries, supporting WGMs, have been extensively studied for more than four decades now. However, the efficient coupling to WGMs mostly rely on experimentally challenging schemes including prism coupling, optical fiber half coupling (OFHC) or free space coupling. This thesis consists of the excitation of silicon microsphere WGMs using an alternative coupling method: shallow waveguides fabricated by femtosecond laser inscription. The evanescent field coupling from the guided modes of the femtosecond micromachined glass and diamond waveguides has been used to excite microsphere WGMs. Furthermore, this thesis includes the excitation of a diamond sphere using an OFHC. Employment of diamond material in photonic applications is substantial, because among all materials, diamond exhibits unique optical properties such as its color centers, large band-gap, high Raman gain, as well as a unique crystal lattice, and robust physical properties. Utilizing diamond as an excitation waveguide material or the cavity material opens the way for combination of both diamond's and WGMs' unique properties for applications in electronics, quantum information processing, and sensing.

ÖZET

Fısıldayan dalga kipleri (FGK), ışığın dielektrik ve simetrik bir çınlacın içerisinde yüzeylerden sürekli yansımaya uğrayarak yerelleşmesiyle oluşan çınlamalardır. Çınlaçların içerisindeki fotonların uzun yaşam süreleri ile sağlanan yüksek nitelik katsayıları, ve dar bant genişlikleri, ve kiplerin çınlaçların içinde çok küçük hacimlere sıkışması gibi benzersiz optik özelliklerinden dolayı, FGK taşıyabilen çınlaçlar kırk yılı aşkın süredir araştırma konusu olmuştur. Ancak, FGK çınlaçlarının etkili bir biçimde optik olarak uyarılması, deneysel olarak gerçekleştirilmesi güç yöntemlerle sağlanmaktadır. Bu tezde, silisyum mikroyuvar çınlaçların uyarılması için değişik bir yöntem olarak femtosaniye lazer ile yazılmış sığ dalgakılavuzları öne sürülmektedir. Femtosaniye lazer ile üretilmiş cam ve elmas dalgakılavuzlarında iletilen kiplerin, kılavuzların dışındaki sönen bileşenleri, mikroyuvarların FGK çınlamalarını uyarmak için kullanılmıştır. Ayrıca, elmas bir mikroyuvarın FGK çınlamaları, optik lif yarı-bağlaştırıcı (OLYB) kullanılarak uyarılmıştır. Elmas, diğer gereçler arasında, renk özekleri, geniş bant aralığı, ve Raman kazancı gibi optik özelliklerinin yanı sıra, eşsiz örüt örgüsü ve sağlam dış özellikleri nedeniyle fotonik uygulamalarda kullanılmak için büyük önem taşımaktadır. Elmas bileşenlerin, çınlama uyarılması için veya bir çınlaç gereci olarak kullanılması; elektronik, nicem bilgi işleme, ve algılama uygulamaları gibi alanlarda hem elmasın hem de FGK çınlamalarının eşsiz özelliklerinden aynı anda yararlanılmasının önünü açmaktadır.

ACKNOWLEDGEMENTS

I would like to thank my advisor Prof. Ali Serpengüzel for giving me the chance to work in Koç University Microphotonics Research Laboratory, for his guidance, kindness, and generous help throughout my Master of Science Thesis research.

Then I would like to thank Prof. Alper Kiraz, and Asst. Prof. Onur Ferhanoğlu for participating as committee members in my thesis, and their valuable feedback.

I would also like to thank Koç University Microphotonics Research Laboratory members; Dr. Ulaş Sabahattin Gökay, Mustafa Mert Bayer, Syed Sultan Shah Bukhari, and Nurperi Yavuz for their help in the laboratory, and for the discussions we had.

I would also like to thank our collaborators in Politecnico di Milano and Institute for Photonics and Nanotechnologies, Professor Roberta Ramponi, Dr. Shane Michael Eaton, Dr. Belén Sotillo, and Vibhav Bharadwaj for providing the shallow waveguide femtosecond laser written waveguides and for valuable scientific discussions.

For their endless love and support, I would like to thank my parents, and my brother.

Finally, I would like to acknowledge Türkiye Bilimsel ve Teknolojik Araştırma Kurumu (TÜBİTAK) grant No. 114F312 for their financial support to our research.

Dedicated to my family…

Table of Contents

List of Figures

NOMENCLATURE

a	Radius of the microsphere
b	Impact parameter
c	Speed of light
E	Electric field
E_g	Band-gap of the material
e_e	Reduced electron mass
D	Sphere diameter
H	Magnetic field
h_l	Bessel functions of third kind
I	Laser intensity
j_l	Spherical Bessel functions of the first kind
k	Wave number
L	Angular momentum of the photon
l	Angular momentum (polar) mode number
m	Azimuthal mode number
m_e	Reduced electron charge
N	Refractive index of the surrounding medium
N_1	Refractive index of the cavity
N_{con}	Electron density in the conduction band
N_s	Normalization constant
n	Radial mode number
P_l^m	Associated Legendre polynomials
p	Momentum of the photon
Q	Quality factor
Q_{rad}	Intrinsic quality factor due to radiative losses
Q_{ss}	Intrinsic quality factor due to scattering losses
Q_{cont}	Intrinsic quality factor due to surface contaminants

Q_{mat}	Intrınsic quality factor due to material losses
Q_{ext}	Quality factor due to external coupling losses
r_{equ}	Equatorial radius
r_{pol}	Polar radius
S_0	Waveguide-sphere separation
t	Field coupling coefficient of the coupling scheme
h	Planck's constant
U and V	Scalar Debye potentials
x	Size parameter
α	Attenuation coefficient
α_{avl}	Avalanche ionization coefficient
B	Surface inhomogeneities' correlation length
β	Ellipticity of sphere
γ	Keldysh parameter
γ_{wg}	Evanescent field decay constant of the waveguide
$\Delta\beta$	Difference of propagation constants
$\Delta\lambda$	Spectral mode spacing
$\delta\lambda$	Resonant peak spectral linewidth
ε_0	Permittivity of the free space
η	Avalanche ionization rate
θ_{in}	Angle of the incident ray
$\theta_{critical}$	Critical angle for total internal reflection
κ	Transfer of field amplitude from the waveguide to the sphere
λ	wavelength of the incident light
σ	Surface inhomogeneities' rms size
ν	Frequency of photon
ω	Angular frequency of photon
ω_0	Resonant angular frequency of an unperturbed sphere

Chapter 1

INTRODUCTION

Whispering Gallery Mode (WGM) resonances, exploit two well-known properties of waves: Reflection and interference. Waves traveling at the surface of a circular cavity go through continuous total internal reflection (TIR) around the surface of the cavity on an equatorial plane. If the optical path of the waves for one round trip is equal to integer number multiples of the wavelength, these waves go through constructive interference, and their amplitudes are added together, forming standing waves, i.e. resonances.

The first scientific paper on, and the first concrete description of the whispering gallery modes (WGMs) was made by Lord Rayleigh (John William Strutt) in 1910, where he investigated the acoustic wave WGMs in the interior dome of St. Paul's Cathedral in London [1]. There are many more historical examples of acoustic whispering galleries around the world, where the sound generated at close proximity of the circular structure result in resonance of the sound waves around the surface, including Temple of Heaven in Beijing, China, Gol Gumbaz in Bijapur, India, and Victoria Memorial in Kolkata, India, which are later studied by Sir Chandrasekhara Venkata Raman [2].

The WGM resonances of electromagnetic waves, which occur on the spherical surface of the dielectric or semiconductor resonators, exhibit unique properties like confinement of the modes in a very small volume, and high power density, as well as long photon lifetime and high quality-factors (Q-factors), due to minimal reflection losses and potentially low material absorption loss [3]. After the proposal of electromagnetic wave WGMs confined on the surface of a dielectric cavity by R.D. Richtmyer [4] in 1939, Garrett et. al. used spherical microcavities as laser resonators in 1961 [5]. With the advancement of experimental and spectroscopic techniques, optical WGM spectra of different materials with different geometries are now extensively studied for more than four decades [6,7].

The WGMs of various geometries such as microdisks [8,9], microrings [10], photonic crystals [11], micropillars [12,13], microtoroids [14], and microspheres [15], which are the simplest three dimensional form to exhibit WGMs [16], are studied. Depending on their optical or electrical properties, or their compatibility with existing technologies, many different materials are used as WGM Resonators, including silica glass [17], silicon [18], $LiNBO_3$ [19], diamond [20], and liquid droplets [21].

High Q-factor WGM resonators are of importance due to their unique optical properties are utilized in many applications as laser resonators [22], tunable optical frequency combs [23], optical channel add-drop filters [24], and label free biosensors of single molecules. Furthermore, the extremely localized resonant modes give rise to non-linear effects in WGM resonators such as, optical parametric oscillations [25], Raman Scattering [26], and Brillouin Scattering [27].

Femtosecond laser micromachining allows removal or property change of either transparent or absorptive materials [28]. In transparent materials, high-energy-density femtosecond laser illumination can be used to induce refractive index change through multiphoton absorption [29]. By photo-inducing different refractive index lines by this technique, permanent waveguides have been written into transparent bulk materials including various glasses [30], and diamond [31]. Femtosecond micromachining found further investigated for fabricating 3D optical memories [32], optical couplers [33], photonic crystals [34], and microfluidic devices [35]. Due to its properties like the need of less expensive and simpler devices, simplicity and high-speed of prototyping, and being intrinsically three-dimensional, i.e., ability to fabricate structures at different depths; femtosecond micromachining is advantageous comparing to other existing manufacturing techniques [36].

Microsphere WGM excitation geometries range from prisms for free-space coupling [37] to optical waveguides such as fiber prisms [38], optical fiber half couplers (OFHCs) [39], ion-exchange waveguides [40], and silicon-on-insulator (SOI) waveguides [41]. In this thesis, we report on excitation of microsphere WGMs using femtosecond micromachined waveguides on glass and diamond bulk materials.

Chapter 2

SPHERICAL MICROCAVITY MODES

2.1. Introduction

Although there are many different cavity geometries to study, whispering gallery modes (WGMs), the simplest mathematical solutions, and the experimental realizations in this thesis belong to spherical resonators. WGMs inside a spherical cavity can be expressed by the rays travelling inside a spherical cavity experiencing total internal reflection (TIR) at each boundary, they face. Considering a light ray hitting a boundary of two surfaces with different refractive index; the ray is reflected from the surface, when the relation:

$$\theta_{in} \geq \theta_{critical} = \arcsin(N/N_1), \tag{2.1}$$

is satisfied, where θ_{in} is the angle of the incident ray, $\theta_{critical}$ is the critical angle for total internal reflection (TIR), N_1 is the refractive index of the cavity, and N is the refractive index of the outside medium. Due to the symmetry of the cavity, reflected light ray will face the boundary again at another point with θ_{in}, resulting in continuous total internal reflection (TIR).

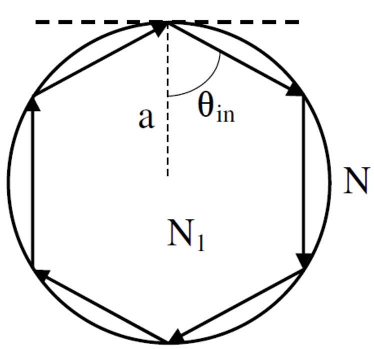

Fig. 2.1 Propagation of a right ray through continuous TIR around a surface of a spherical cavity.

If the incident angle θ_{in} of the reflected light is approximately $\pi/2$ (near-glancing incidence), the beam propagation is close to the surface of the sphere. If the optical path of the light ray is equal to an integer multiple of the wavelength, the constructive interference occurs. The condition for the resonance is thus,

$$2\pi a = (\lambda / N_1) l \, , \tag{2.2}$$

where a is the radius of the sphere, λ is the wavelength of the light, and l is an integer (angular momentum number). As it can be seen from the Fig. 2.2, if we consider that, the incident ray is a photon, one can deduce the relation of l with the angular momentum of the resonant photon as [3],

$$L \approx ap = \frac{ah}{\lambda} = \frac{hl}{2\pi} \, , \tag{2.3}$$

where h is the Planck's constant, p the momentum of the photon, and L the angular momentum of the photon. For the sphere with a radius $a >> \lambda$, the WGMs are described as high angular momentum electromagnetic modes, where the light propagation around the sphere is maintained by continuous total internal reflection (TIR).

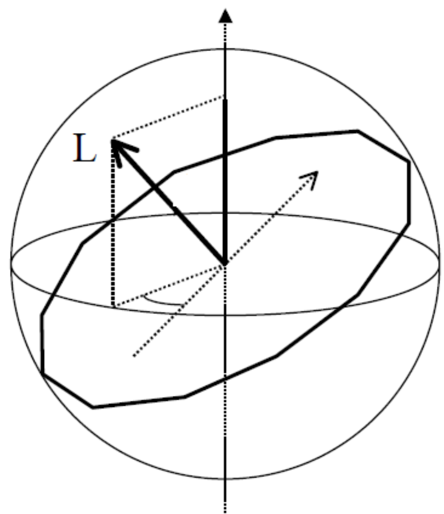

Fig. 2.2 Angular momentum **L** of a photon travelling around a sphere.

For the accurate and complete explanation of the WGMs, the wave nature of the light has to be taken into account.

2.2. Microsphere WGMs

In order to find the field solutions of WGMs of a microsphere, we need to find the solutions to the Maxwell's equations inside a spherical cavity for the transverse electric polarization (TE), of which the electric field component is tangent to the surface of the sphere and perpendicular to the direction of propagation, and transverse magnetic (TM) polarization, where the magnetic field component is tangent to the surface of the sphere and perpendicular to the direction of propagation. In order to solve the Maxwell's equations, scalar Debye potentials are used [42,43] in order to get the equations:

$$\frac{\partial^2 U}{\partial r^2}+\frac{1}{r^2\cos\theta}\frac{\partial}{\partial\theta}\left(\cos\theta\frac{\partial U}{\partial\theta}\right)+\frac{1}{r^2\cos^2\theta}\frac{\partial^2 U}{\partial\phi^2}+k^2U=0\,,\quad \text{for TM Modes,} \tag{2.4}$$

$$\frac{\partial^2 V}{\partial r^2}+\frac{1}{r^2\cos\theta}\frac{\partial}{\partial\theta}\left(\cos\theta\frac{\partial V}{\partial\theta}\right)+\frac{1}{r^2\cos^2\theta}\frac{\partial^2 V}{\partial\phi^2}+k^2V=0\,,\quad \text{for TE Modes,} \tag{2.5}$$

where V and U are scalar potentials and k is the wave number, which is equal to ω/c. The resulting electric and magnetic fields are than found as follows:

$$E_r=\left(\frac{\partial^2}{\partial r^2}+k^2\right)U\,,\qquad H_r=0\,, \tag{2.6}$$

$$E_\theta=\frac{1}{r}\frac{\partial^2 U}{\partial r\partial\theta}\,,\qquad H_\theta=-ik\frac{1}{r}\frac{\partial U}{\partial\phi}\,, \tag{2.7}$$

$$E_\phi=\frac{1}{r\cos\theta}\frac{\partial^2 U}{\partial r\partial\phi}\,,\qquad H_\phi=ik\frac{1}{r}\frac{\partial U}{\partial\theta}\,, \tag{2.8}$$

for the TM modes, and

$$H_r = \left(\frac{\partial^2}{\partial r^2} + k^2 \right) V , \qquad E_r = 0 , \tag{2.9}$$

$$H_\theta = \frac{1}{r} \frac{\partial^2 V}{\partial r \partial \theta} , \qquad E_\theta = -ik \frac{1}{r} \frac{\partial V}{\partial \phi} , \tag{2.10}$$

$$H_\phi = \frac{1}{r \cos\theta} \frac{\partial^2 V}{\partial r \partial \phi} , \qquad E_\phi = ik \frac{1}{r} \frac{\partial V}{\partial \theta} , \tag{2.11}$$

for the TE modes. Note that the field solutions for each spherical axis are separable and can be expressed as:

$$\Psi_{nlm}(r,\theta,\phi) = N_s \psi_r(r) \psi_\theta(\theta) \psi_\phi(\phi) , \tag{2.12}$$

where Ψ is the electric or magnetic fields in the case of TE or TM modes respectively, and N_s is a normalization constant. The subscript n denote the radial mode number, whereas the subscript l denotes the polar mode number, and the subscript m denotes the azimuthal mode number, found from the boundary conditions. The difference l-$|m|$ is the polar mode order. From the above equations, the differential equations for the fields' dependences on the spherical coordinates can be found as [44]:

$$\frac{d^2}{dr^2}\psi_r + \frac{2}{r}\frac{d}{dr}\psi_r + \left(k^2 n_s^2 - \frac{l(l+1)}{r^2} \right) \psi_r = 0 , \tag{2.13}$$

$$\frac{1}{\cos\theta}\frac{d}{d\theta}\left(\cos\theta \frac{d}{d\theta}\psi_\theta \right) - \frac{m^2}{\cos^2\theta}\psi_\theta + l(l+1)\psi_\theta = 0 , \tag{2.14}$$

$$\frac{d^2\psi_\phi}{d\phi^2} + m^2 \psi_\phi = 0 . \tag{2.15}$$

The solutions to these differential equations are found to be:

$$\psi_r(r) = \begin{cases} j_l(kN_1 r), & r \le a \\ h_l(kN_1 r), & r > a \end{cases} \tag{2.16}$$

$$\psi_\theta(\theta) = P_l^m(\sin\theta)\,, \qquad (2.17),$$

$$\psi_\phi(\phi) = e^{\pm im\phi}\,, \qquad (2.18).$$

where j_l and h_l are the spherical Bessel functions of the first kind, and Bessel functions of the third kind (spherical Hankel functions), respectively. P_l^m denote the associated Legendre polynomial.

For different polar and azimuthal mode numbers, the angular dependence of the field distributions is analogous with the spherical harmonic functions. For a sphere with a fixed radius, each polar mode number (angular momentum number) corresponds to a certain wavelength. For a polar mode number l, there are $(2l+1)$ allowed field distributions for each azimuthal mode number ($m = -l, \ldots, 0, \ldots, l$).

2.3. Microsphere WGM Spectra

In order to investigate the WGM spectra of a microsphere, the general method is to measure scattering signal at different wavelengths. WGMs in microspheres result in high power densities to be confined in very small regions. A portion of this power will be scattered out from the sphere due to Mie scattering, resulting in sharp peaks in the scattering spectra at the wavelength corresponding to certain mode number and mode orders. WGM peaks quantized by their angular momentum number l exhibit themselves in distinct modes for TE and TM polarized fields, separated by a spectral mode spacing $\Delta\lambda$ (the analogue of the Fabry-Pérot resonator’s free-spectral-range (FSR)) for the resonances with consecutive polar mode numbers, and defined according to the Lorenz-Mie theory [45] as:

$$\Delta\lambda = \frac{\lambda^2 \tan^{-1}\sqrt{\left(\frac{N_1}{N}-1\right)}}{2\pi a\sqrt{\left(\frac{N_1}{N}-1\right)}}\,, \qquad (2.19)$$

where λ is the wavelength of operation. Exemplary scattering spectra of resonances of microspheres with different excitation geometries can be found in the next chapters, where the experimental results are presented.

TE and TM modes with consecutive *l* numbers are separated with mode spacing $\Delta\lambda$. Note that, there is a shift between identical TE and TM spectra; this is due to the relative phase shifts experienced by TE and TM waves going through total internal reflection (TIR). This shift is given by [46]:

$$\Delta \nu_{n,l}^{TE,TM} \simeq \frac{c}{2\pi Na} \frac{\sqrt{N^2-1}}{\sqrt{N}} . \tag{2.20}$$

For a perfectly round sphere, different mode orders l-$|m|$ for a polar mode number l correspond to the exact same frequency. Thus, the TE and the TM modes in a perfect sphere are said to be $(2l+1)$-fold degenerate for each azimuthal mode number m [47]. However, for an eccentric spheroid, the degeneracy of the sphere WGM modes is lifted due to the broken spherical symmetry. In a spheroid with different polar and equatorial radii, different mode orders for the same polar mode number l are seen as side-peaks at different frequencies. The azimuthal mode number dependent frequencies of these modes can be obtained from [47]

$$\omega(m) = \omega_0 \left[1 - \frac{\beta}{6} \left(1 - \frac{3m^2}{l(l+1)} \right) \right], \tag{2.21}$$

where ω_0 denotes the angular frequency of the unperturbed sphere, β denotes the ellipticity as,

$$\beta = \frac{\left(r_{pol} - r_{equ} \right)}{r_{eff}} , \tag{2.22}$$

where r_{pol}, and r_{equ} are the polar and the equatorial radii, respectively, and the effective radius r_{eff} is given as:

$$r_{eff} = \left(r_{equ}^2 r_{pol}\right)^{1/3}. \tag{2.23}$$

2.3.1. Quality Factor

Fig. 2.3 shows the high resolution spectrum of a single peak in WGMs of a microsphere analyzed in Chapter 6. The full-width-at-half-maxima (FWHM) of the single peak is denoted as δλ, and is also the linewidth of this resonance peak. The quality factor (*Q-factor*) of the WGM is found using the relation:

$$Q = \frac{\lambda}{\delta\lambda}. \tag{2.24}$$

One of the unique properties of WGM resonators are their very high quality factors, due to their long photon lifetime and low cavity losses; which makes them crucial for applications such as and wavelength division multiplexing (WDM), [48] and cavity quantum electrodynamics (QED) experiments [49].

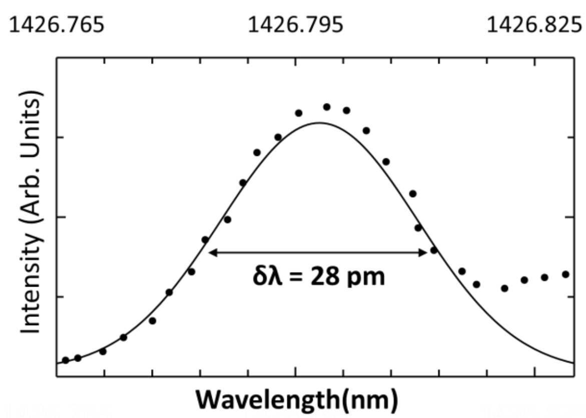

Fig. 2.3 The resonance wavelength and linewidth of a single WGM peak in a elastic scattering spectrum from a diamond microsphere on a silica optical fiber half coupler (OFHC).

The quality factor of WGMs depend on different properties of the cavity material, the surrounding medium, and the coupling mechanisms. These factors, which limit the ultimate Q-factor of WGMs can be summarized as [50,51]:

$$Q^{-1} = Q_{rad}^{-1} + Q_{ss}^{-1} + Q_{cont}^{-1} + Q_{mat}^{-1} + Q_{ext}^{-1}, \tag{2.25}$$

where Q_{ext} is caused by the external coupling losses, and depends on the coupling mechanism and geometry, Q_{rad} is due to intrinsic radiative (curvature) losses of the cavity, Q_{ss} is caused by scattering losses due to residual surface inhomogeneities, Q_{cont} is introduced by surface contaminants, and Q_{mat} is due to material loss.

Q_{rad}^{-1} is due to the curvature of the WGM resonator, and vanishes exponentially with increasing radius of curvature. This radiative component of the Q-factor can be neglected for the spheres with $a/\lambda \geq 15$, resulting in quality factors larger than 10^{11}.

Small fraction of the photons going through total internal reflection (TIR) under grazing incidence experiences Rayleigh scattering by surface clusters having the size of single molecules. These scattered photons have a limitation effect on the quality factor, expressed as:

$$Q_{ss} = \frac{\lambda^2 D}{2\pi^2 \sigma^2 B}, \tag{2.26}$$

where B denotes the surface inhomogeneities' correlation length, and σ the surface inhomogeneities' rms size, respectively. The principal limit for the quality factor of large spheres in the absence of contaminants are defined by the material losses, expressed as:

$$Q_{mat} = \frac{2\pi n}{\alpha\lambda}, \tag{2.27}$$

where α is the attenuation coefficient of the cavity material at a wavelength λ. Q_{ext} is the contribution of the coupling losses to the total quality factor of WGMs. Assuming the field coupling coefficient of the used coupling scheme is t [51], the Q_{ext} can be expressed as:

$$Q_{ext} = \frac{(2\pi)^2 a}{\lambda |t^2|}. \tag{2.28}$$

2.4. Coupling to Microsphere WGMs

Applications of WGMs in microspheres depend largely on the successful coupling to the WGMs. There are several coupling mechanisms in order to achieve coupling to WGMs of microspheres.

Tapered fibers are fabricated by heating and stretching an optical fiber from both ends. The narrow fiber waist allows the evanescent tail of the guided mode to be coupled to WGM modes in the presence of a microsphere in close proximity of the tapered fiber. This mechanism suffers from fragility of the tapered fiber, of which the waist can be reduced down to the micrometer scale [52].

Prism coupling is the oldest coupling method, using frustrated total internal reflection (*frustrated*-TIR) from the reflected light at the boundary of the prism [53]. Prism coupling can be further improved in terms of compactness using angle polished fiber-prism [38].

Buried glass channel waveguides are used for coupling to WGMs of microspheres. Robustness and compatibility with planar lightwave circuits (PLCs) provides advantage of the buried waveguides, which trades off the coupling efficiency [40].

This work focuses on femtosecond laser micromachined waveguide excitation of microsphere WGMs. The guided mode going through the femtosecond laser micromachined waveguides can be approximated to have a Gaussian beam profile [54]. The evanescent wave coupling to microsphere WGMs thus, can be analyzed in a manner similar to the tapered fiber and half-block couplers.

For the excitation of microsphere WGMs using femtosecond laser written waveguides, the coupling factor κ denotes the amplitude transfer coefficient from the waveguide to the sphere per one revolution. Similarly, κ^2 is the power transferred from the waveguide to the sphere per one revolution, and can be expressed as [55]:

$$\kappa^2 = \kappa^2\left(S_0\right)\frac{2\pi a}{\gamma_{wg}}\exp\left(\frac{-a\Delta\beta^2}{\gamma_{wg}}\right), \tag{2.29}$$

where $\Delta\beta$ is the difference in propagation constants between waveguide mode and the sphere mode, γ_{wg} the evanescent field decay constant of the waveguide away from the waveguide surface. $\kappa^2(S_0)$ is the interaction strength between the waveguide mode and the sphere mode at the minimum separation S_0 between the waveguide axis and the surface of the sphere, and can be expressed with the field overlap integral:

$$\kappa^2\left(S_0\right) = \frac{\pi}{N_1\lambda}\int\int_{sphere}\left(N_1^2 - N^2\right)E_w\Psi_{nlm}dxdy, \tag{2.30}$$

where E_w denotes the waveguide mode, and Ψ_{nlm} denotes the sphere mode field distribution, which depends on the mode numbers *n*, *l*, and *m* [55].

2.4.1. Impact Parameter

The characteristics of the microsphere WGM excitation can be identified through the localization principle [56], which relates the impact parameter b_l of the excitation light ray with the angular-momentum quantum number *l* of the WGM as,

$$b_l = \frac{\left(l + 1/2\right)\lambda}{2\pi}. \tag{2.31}$$

This relationship, together with the generalized Lorenz-Mie theory (GLMT) [57], which gives an applicable solution for excitation with a Gaussian beam, yields a range for impact parameters as:

$$(a \le b \le \left(N_1/N\right)a), \tag{2.32}$$

with corresponding mode numbers,

$$(x \le l \le \left({N_1}/{N} \right) x), \tag{2.33}$$

which are able to excite the microspheres WGMs [58]. In this case, the size parameter is defined as:

$$x = 2\pi a N / \lambda \ , \tag{2.34}$$

and the impact parameter *b* is defined as the distance from the center of the excitation beam inside the waveguide to the center of the microsphere.

Fig. 2.4 [59] shows the geometrical interpretation of coupling to the microsphere WGMs using a waveguide carrying a Gaussian beam. The impact parameter might be a way of quantifying how many WGMs can be excited. The excitation impact parameter depends on the size of the sphere, as a larger sphere has a greater impact parameter, i.e., WGMs with higher mode numbers can be excited.

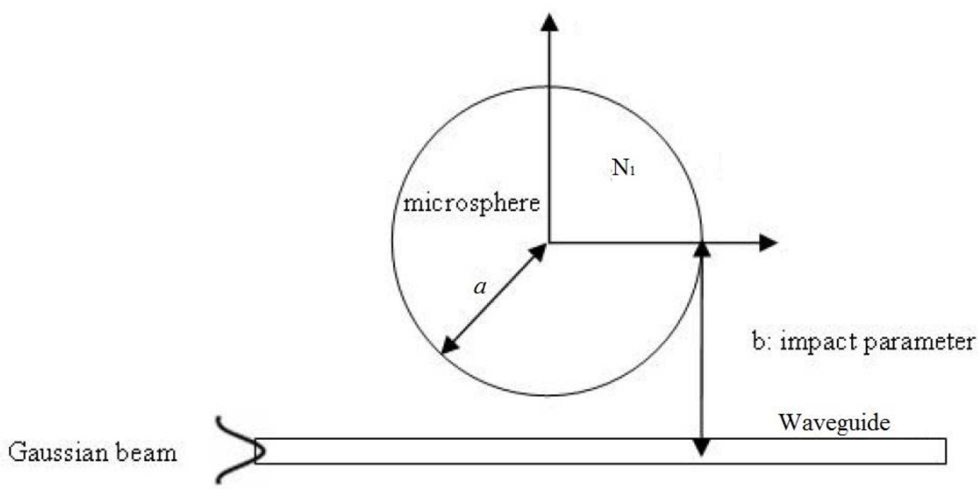

Fig. 2.4 Schematic illustration of a microsphere coupled to a waveguide placed at an impact parameter *b* away from the microsphere center.

Chapter 3

FEMTOSECOND LASER MICROMACHINING

3.1. Introduction

Since the advent of the high-power pulsed lasers, nonlinear response of the materials, and optically induced breakdown in such bulk media have been studied extensively for more than half a century [60]. With the femtosecond laser pulses, producing the power needed for the nonlinear absorption in dielectric materials, giving rise to the confinement of the incident laser at micrometer level inside the bulk material, photoinduced property or morphology change in small volumes have been an active area of research. Depending on the laser illumination parameters such as energy, pulse duration, and repetition rate, as well as the material properties like electronic bandgap, and thermal conductivity, modifications on the exposed volume range from small refractive index changes to the birefringent, periodic nanoplanes, which can be etched chemically to form microfluidic channels, and empty voids caused by microexplosions inside the material. By changing the laser focus relative to the sample, photonic structures and devices can be formed in arbitrary 3D shapes, improving the traditional fabrication techniques such as photolithography, which is inherently planar [61].

3.2. Femtosecond Laser Pulse-Material Interaction

Even though the complete model for the laser-material interaction is yet to be discovered, main mechanism for the femtosecond laser induced modification of the materials can be reduced to the main steps of free electron plasma formation inside the material, transfer of the energy (relaxation) to the surrounding media and formation of modifications [62].

3.2.1. Free Electron Plasma Formation

In the transparent dielectric materials, electrons tend to occupy the valence band energy level, which is the lowest band of allowed states. An energy gap separates the valence band from the conduction band. If the electron in the valence band gains enough energy, i.e., energy greater than the energy gap between the valence and the conduction bands, they can be promoted to become free electrons. Typically, nonlinear absorption of visible or near-infrared light is not sufficient for such a transition. However, in the presence of high-intensity femtosecond laser pulses, the plasma formation is achieved through nonlinear laser absorption, which promotes the electrons from valence band to the conduction band. Photoionized electrons induce permanent changes in the material by transferring their energy to the lattice [63]. Nonlinear photoionization is dominated by two mechanisms, namely, photoionization and avalanche ionization [64].

In photoionization process, depending on the incoming photon energy, the electrons in the valence band are promoted to the conduction band. There are two main mechanisms for photoionization, which are multiphoton ionization, and tunneling ionization. Simultaneous absorption of two or more photons leads to releasing of electrons from the material. For incoming photons having smaller frequency, but still having the energy to distort the Coulomb field experiences by the electron, the electron is allowed to tunnel out of its bound state. A theoretical framework for these processes introduces a parameter γ, known as the Keldysh parameter [65], determining the dominating photoionization process. The Keldysh parameter is given by:

$$\gamma = \frac{\omega}{e_e}\sqrt{\frac{m_e c N_b \varepsilon_0 E_g}{I}}\ , \tag{3.1}$$

where ω denotes the laser frequency, m_e and e_e the reduced electron mass and charge, c the speed of light, N_b the refractive index of the material, E_g the band-gap of the material, and

ε_0 is the permittivity of free space. The Keldysh parameter is $\gamma > 1.5$ for multiphoton ionization, and $\gamma < 1.5$ for tunneling ionization to be predominant. For $\gamma = 1.5$, both multiphoton and tunneling ionization contribute to the ionization process.

Avalanche ionization involves free-carrier absorption followed by impact ionization. When an electron in the conduction band further absorbs laser light (linear absorption is allowed in this part), moving to a higher energy state at least E_g higher than the lowest conduction band energy, it can collisionally ionize (impact ionization) a neighboring electron from the valence band. This process results in two electrons in the lowest energy level of the conduction band. As long as there is a laser field present, the electron density, N_{con}, in the conduction band grows exponentially according to:

$$\frac{dN_{con}}{dt} = \eta N_{con} \quad , \tag{3.2}$$

where η is the avalanche ionization rate [66]. In the model developed by Stuart et al. for the avalanche ionization, the avalanche ionization rate depends linearly on the laser intensity (I) [67] as,

$$\eta = \alpha_{avl} I \quad , \tag{3.3}$$

where α_{avl} is the avalanche ionization coefficient.

3.2.2. Material Modification

After the free electron plasma creation, the physical mechanism for formation of different structural changes is not fully understood. However, depending on the laser and material properties, modification of exposed regions can be divided into three different types; a smooth isotropic refractive index change, a birefringent refractive index change, and a void.

For laser pulse energies just above the modification threshold level, a smooth refractive index change is induced in the material. One of the most accepted mechanism for this modification is due to the energy deposited into the focal volume leads to local rapid heating of a small volume at the local spot [68]. A thermal gradient localized at the focal point is induced in the material by this process, the material cools down rapidly. Due to this rapid heating and cooling, either increased or decreased refractive index formed inside the material with increasing cooling rates, confirming the relation of the process with heating [63]. It has also been proposed that, the radiation produces color centers to change the refractive index through a Kramers-Kronig mechanism [69]. Another approach for the refractive index altering in femtosecond laser exposure is that, the densification and strain in the material due to the stress, that is produced in the surrounding medium due to exposed region's volume change[70]. Since each mechanism is proven to have an effect in the refractive index change, this modification is likely produced by the combination of heating, color center production, and densification inside the material.

Using slightly different laser illumination parameters, nanoporous structures, which align themselves periodically (with the period of as low as tens of nanometers) in the perpendicular direction to the electric field component of the linearly polarized femtosecond laser beam, are created [71]. These periodic nanostructures consist of slightly varying density regions, giving rise to birefringent refractive index changes [72]. These structural changes has been only realized in fused silica, and are the smallest embedded structures, which are created using light [63].

At higher energy femtosecond laser pulses, the formation of free electron plasma occurs due to the avalanche ionization and continuous impact ionization. As the temperature of the focal point increases up to a level, where the plasma causes a charge separation enough to cause Coulomb explosion (microexplosion), generated shock wave carries the matter and energy away from the exposed point, creating a less dense area or a hollow core, namely a void [73]. Microfluidic channels [74], optical waveguide arrays [75], and optical memory devices [76] were reported to be fabricated by void formation in bulk materials using femtosecond lasers.

In summary, the key steps in formation of structural changes using femtosecond laser illumination are as follows. First, a free electron plasma is formed in the focal volume due to nonlinear absorption. Then, three different modification types are induced in the material depending on the energy contained in the plasma; smooth refractive index change, birefringent refractive index change, and void formation [74].

Chapter 4

EXCITATION OF Si SPHERE WGMs WITH FEMTOSECOND LASER WRITTEN GLASS WAVEGUIDES

In this chapter, experimental results regarding the excitation of WGMs of a silicon (Si) microsphere having a radius of 500 μm, using a 25 μm deep femtosecond laser inscribed glass optical waveguide, having a large mode field diameter (MFD) in the near-infrared (near-IR) region, are presented. The resonance spectra of silicon sphere WGMs, which exhibit quality factors of approximately 10^5, show that femtosecond laser inscription on dielectric materials can be an alternative method for producing a reliable platform for coupling to the WGMs of the microspheres. Excitation of WGMs in microresonators by overlapping the evanescent fields from fs laser fabricated optical waveguides may offer more robustness and reliability in photonic applications.

4.1. Gorilla Glass Waveguides

Femtosecond (fs) laser inscribed shallow glass waveguides are fabricated with different parameters to optimize the coupling to microsphere WGMs. These waveguides are later on characterized in order to examine their eligibility for evanescent field coupling to microspheres. The optical waveguides were fabricated in the bulk glass (Corning, Gorilla) (with dimensions of 5 cm x 5 cm x 0.1 cm) by using a femtosecond pulsed laser (Pharos, Light Conversion) using the fundamental wavelength of 1030 nm and a repetition rate of 500 kHz. The objective was to produce optical waveguides with high transmission at 1550 nm with a large MFD at a shallow depth to allow for the most efficient evanescent coupling to the surface microspheres. The femtosecond pulsed laser was focused to

20-25 μm below the surface of the glass using a 0.42 NA objective. At shallower depths, no waveguide structure can be formed, as the surface of the glass is ablated by the femtosecond laser, thus becoming non-guiding, and scattering the input light to the outside medium. The processing window for obtaining low loss waveguides (propagation losses below 1 dB/cm) with a large mode field diameter (MFD > 17 μm) were an average laser power of 325 to 375 mW and a scan speed of 2 to 20 mm/s. The MFD parameter results obtained by measuring the near field intensity profile of the waveguides fabricated with different laser powers (P), scan speeds (v), and at different depths at 1550nm wavelength are shown in Table 4.1 and Table 4.2. The results indicate single mode (SM) guiding with vertical and horizontal mode field diameters are indicated in brackets.

	P (mW)		
v (mm/s)	**325**	**350**	**375**
2	SM (17x21)	SM (17x22)	SM (19x26)
5	SM (18x22)	SM(17x22)	SM (18x23)
10	SM (21x24)	SM (19x23)	SM (19x24)
15	SM (24x27)	SM (21x24)	SM (19x24)
20	SM (28x30)	SM (22x26)	SM (20x24)

Table 4.1 Mode Field Diameter (MFD) measurements of shallow waveguides with different parameters at a depth of 20 μm

For the excitation of silicon microsphere WGMs, the femtosecond laser written waveguide fabricated at a depth of 25 μm with an average power of 350 mW and a scanning speed of 2 mm/s is chosen. Fig. 4.1 below shows the (a) top view, (b) side view and (c) near-field intensity profile of the selected waveguide. As seen in Fig. 4.1(c), the near field intensity profile of the waveguide at 1550 nm wavelength shows single mode guiding. Therefore, we treat our coupling to the Si microsphere and scattering from the Si microsphere as excited by a single mode waveguide. From the side view, the transmission optical microscope image of the waveguide fabricated at 25 µm depth with an average power of 350 mW and a scanning speed of 2 mm/s (Fig. 4.1.(b)) we see that, the upper boundary is at a depth of about 10 µm below the surface. The $1/e^2$ intensity of the MFD of this waveguide is 22 µm by 17 µm in the vertical and transverse direction, respectively. The large mode size of the femtosecond written glass waveguide enables evanescent coupling with a microsphere placed on the surface. The propagation loss for this Gorilla glass waveguide was 0.8 dB/cm at 1550 nm wavelength.

	P(mW)		
v (mm/s)	**325**	**350**	**375**
2	SM (17x21)	SM (17x22)	SM (18x25)
5	SM (19x23)	SM(16x19)	SM (19x25)
10	SM (21x26)	SM (19x24)	SM (20x25)
15	SM (25x28)	SM (21x25)	SM (21x25)
20	SM (29x32)	SM (23x27)	SM (22x26)

Table 4.2 Mode Field Diameter (MFD) measurements of shallow waveguides with different parameters at a depth of 25 µm

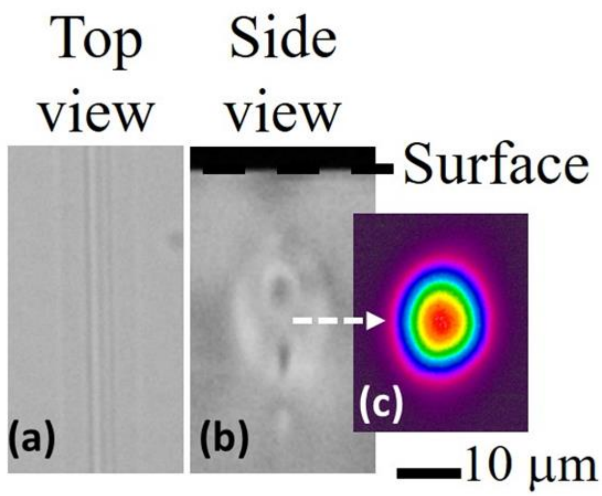

Fig. 4.1. (a) Top view, (b) side view, and (c) near-field intensity profile at 1550 nm wavelength of the fs laser written waveguide fabricated with an average power of 350 mW and a scanning speed of 2 mm/s.

4.2. Experimental Setup

The experimental setup used for fs laser micromachined glass optical waveguide characterization, and coupling to Si microsphere WGMs is shown in Fig. 4.2. The Si microsphere is positioned by a metal tube attached to the sphere by vacuum suction and manipulated by the use of mechanical micrometer stages. The sphere was detached from the suction tube during the excitation by the glass waveguide. The Si microspheres, which are purchased from Ball Semiconductor, were produced by the crystallization of Si melts dropping in free-fall tube through a plasma furnace, and mechanically lapped and polished to make a mirror-like finish with no surface defects and damage [77].

As seen in Fig. 4.2, a red probe laser is fiber coupled to the glass waveguide with a 50/50 coupler, and operates at a wavelength of 637 nm. The red probe laser is used for aid in the alignment of the optical fiber measurement setup. The input and output coupling to the glass waveguide are achieved by end coupling of a cleaved and polished SMF with 8.2 μm core diameter. In order to reduce the stray light and to achieve efficient coupling, we used index matching gel (with refractive index 1.46) at the input and output facets of the waveguide. The red streak along the waveguide is the result of scattering due to the sidewall roughness and inhomogeneities within the fs laser-written waveguide. The nearby ablation lines are also faintly visible due to their scattering of uncoupled light (Fig. 4.2(a)).

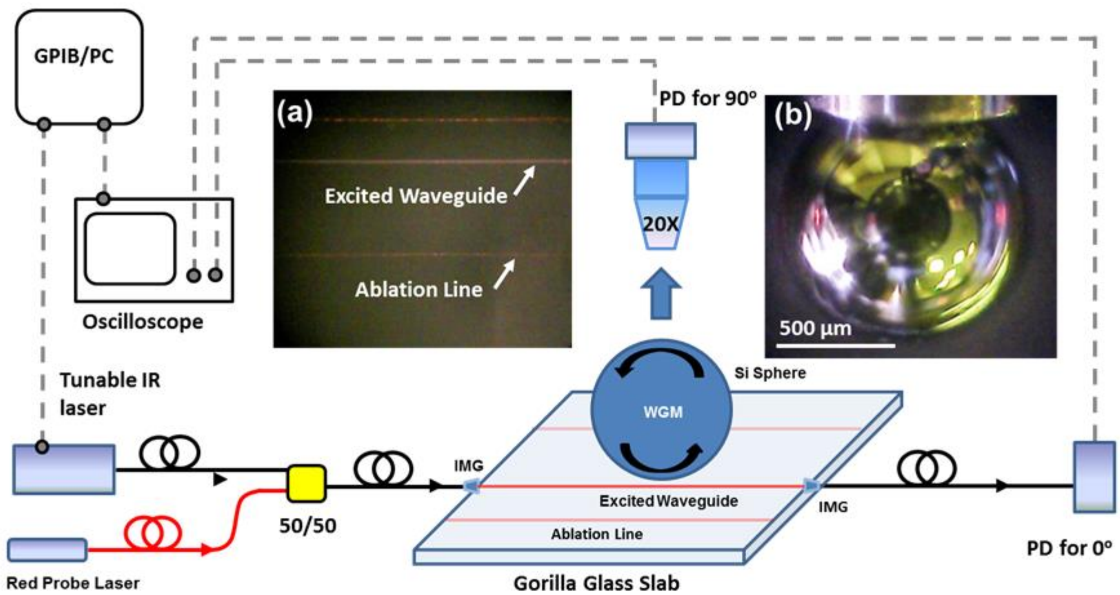

Fig. 4.2. The schematic of the optical setup shows the WGM excitation in Si microsphere by the glass waveguide. The inset shows the top view of (a) the fs laser written Gorilla glass waveguide and ablation line, (b) the Si microsphere held by the metal suction tube. Ablation lines are reference lines fabricated on the surface of glass to aid in the fiber alignment to the faint buried optical waveguides, which are barely visible by optical microscopy.

A narrow linewidth continuous wave (CW) tunable distributed feedback (DFB) laser operating around 1427 nm is used as the excitation source. As the wavelength of the near-IR laser is tuned with a resolution of 1.1 pm, we measured the intensity of the elastic light scattering from a 500 µm radius Si microsphere in both 0° (transmission) and 90° (scattering) angles. Intensity measurements were performed with InGaAs photodetectors (PDs), whose outputs were fed into an oscilloscope with a 100 MHz bandwidth. The analog outputs of the oscilloscope were connected to a PC with IEEE-488 General Purpose Interface Bus (GPIB) for data acquisition.

4.3. Experimental Results

Fig. 4.3 and Fig. 4.4 show the measured light intensities of 90° elastic scattering and 0° transmission signals from the Si microsphere on a glass waveguide fs laser inscribed at 25 μm depth with an average power of 350 mW and scan speed of 2 mm/s. In Fig. 4.3(a), no coupling between the Si microsphere and the glass waveguide is observed, whereas in Fig. 4.3 (b), Fig. 4.4(a), and Fig. 4.4(b), coupling to the WGMs of the Si microsphere is observed. The large MFD of the fs-laser written waveguide and the high refractive index of the Si sphere (3.48) enables the evanescent field coupling between the waveguide and the sphere. The 90° elastic scattering peaks and the 0° transmission dips are due to the coupled near-IR light around 1427 nm. Mixed polarized light from the output of the near-IR laser diode is used. Also mixed polarized scattered light is collected from the WGMs of the microsphere. The calculated value for mode spacing $\Delta\lambda$ between two WGMs with consecutive mode numbers, (due to quantization in polar angular direction) in the same mode order (due to quantization in the radial direction) for the 500 μm Si sphere, is found as 0.248 nm using (2.19). The occurrence of light coupling between the glass optical waveguide and the Si microsphere is manifested in the correlation between calculated and experimental mode spacing of approximately 0.25 nm.

The linewidth of a single peak in the 90º scattering spectrum around 1427 nm is found as $\delta\lambda = 0.0168$ nm, resulting in a WGM quality factor of $Q = 8.5 \times 10^4$. Assuming the intrinsic Q factor of the Si microsphere is dominated by the material absorption losses, its value is given by (2.27), where $\alpha < 0.01$ cm^{-1} is the silicon absorption coefficient [78]. At the operation wavelength of 1427nm, Q_{mat} is 1.5x10^7, i.e., approximately two orders of magnitude higher than the measured Q-factor, which is limited by the linewidth of the DFB laser in our measurement setup.

Fig. 4.3(a) shows the baseline scattering and transmission spectra. In Fig. 4.3(b), multiple WGMs are observed in the scattering, and one WGM is observed in transmission, where the absence of the corresponding scattering peak might be due to destructive multiple WGM interference in the scattering signal at 90º. In Fig. 4.4(a), again multiple WGMs are observed in the scattering, and one WGM is observed in transmission, with corresponding WGM enhancement in scattering signal. In Fig. 4.4(b), multiple WGMs are observed in the scattering, and two WGMs are observed in transmission, with corresponding WGM enhancements in scattering signal. As seen in Fig. 4.4(a) and (b), the coupling efficiency is increased for several WGMs. Since the evanescent coupling is extremely sensitive to the spatial positioning, when coupling to deep Gorilla glass waveguide, changes in the coupling efficiency might be caused by the small variations in the position of the Si microsphere relative to the glass waveguide.

The position of the fs-laser inscribed glass optical waveguide with respect to the center of the Si microsphere, result in a relatively high impact parameter (b = 525 μm) value for microsphere WGM excitation. When compared with the shallower OFHC excitation of a Si microsphere [79],where the impact parameter is close to the radius of the sphere, the excitation of the Si microsphere with a fs-laser written waveguide (at a depth of 25 μm below the surface of the glass) results in a larger impact parameter.

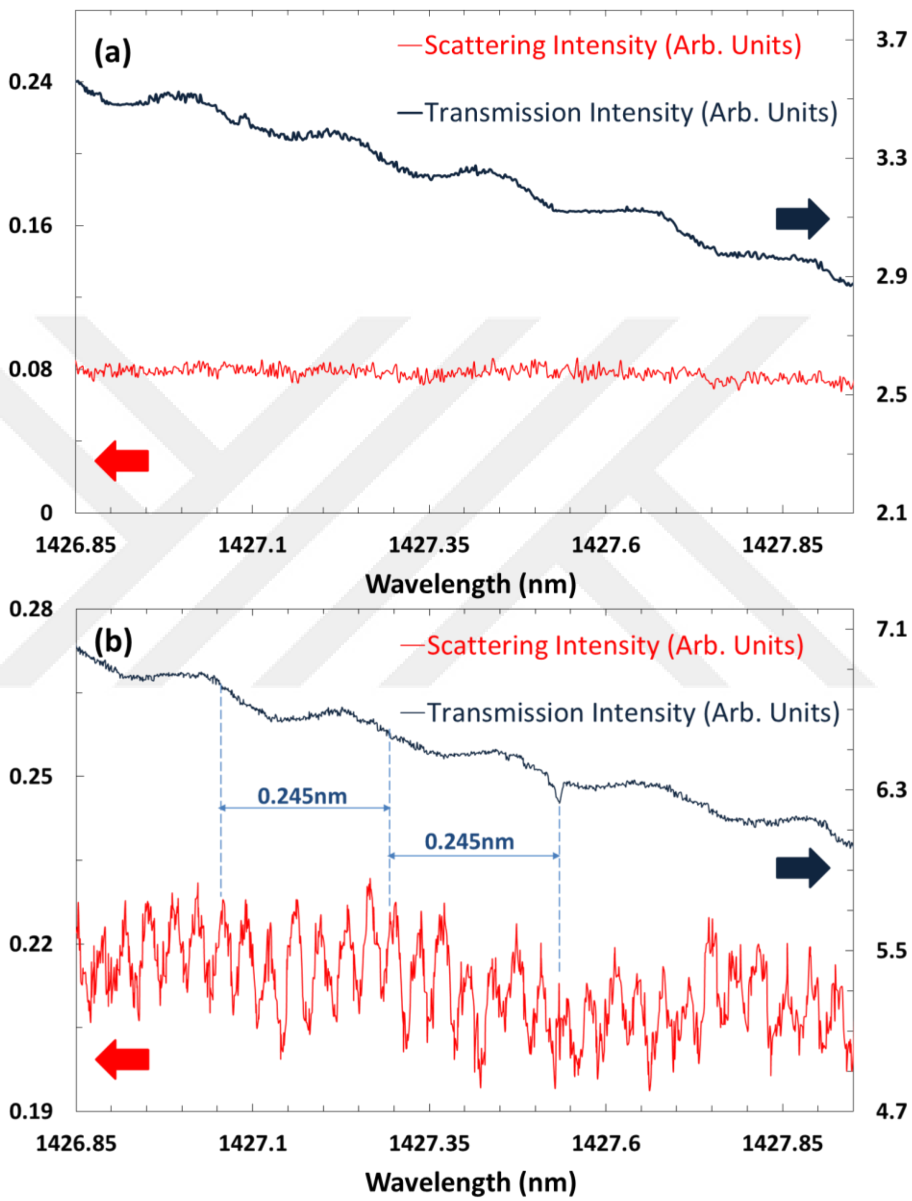

Fig. 4.3. 90º elastic scattering and 0º transmission spectra from the Si microsphere excited with the fs pulsed laser inscribed glass optical waveguide showing (a) no coupling, (b) weak coupling to WGMs of the Si microsphere. The values on the vertical axes denote the scattering (left) and transmission (right) intensities.

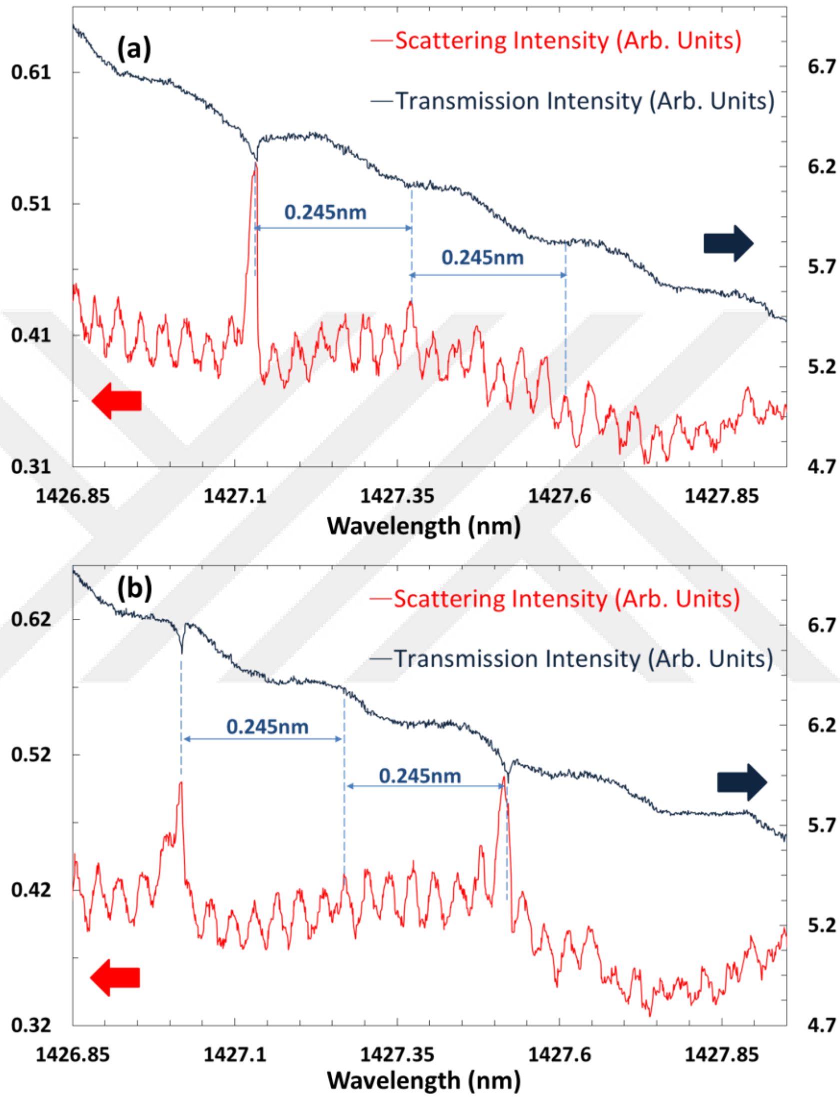

Fig. 4.4. 90º elastic scattering and 0º transmission spectra from the Si microsphere excited with the fs pulsed laser inscribed glass optical waveguide showing (a) stronger coupling to one, and (b) stronger coupling to two WGMs of the Si microsphere. The values on the vertical axes denote the scattering (left) and transmission (right) intensities.

Chapter 5

EXCITATION OF Si SPHERE WGMs WITH FEMTOSECOND LASER WRITTEN DIAMOND WAVEGUIDES

In this chapter, light coupling from a femtosecond laser written shallow diamond waveguide to a silicon microsphere having a radius of 500 μm is presented in the near-infrared (near-IR) region. The WGM spectra exhibits quality factors around 5 x 10^5. Femtosecond laser written diamond waveguides provide a viable platform for WGM excitation of microspheres, enabling the integration, as well as robust realization of devices in the promising area of diamond photonics [80]. The employment of the diamond as the bulk material in photonic applications requires some knowledge about the optical properties of diamond. A brief discussion on the color centers of diamond is given in the next section.

5.1. Color Centers of Diamond

Regarding its wide range of color centers and their controlled detection of electron spin and magnetic resonances, which makes these color centers promising candidates for utilizing as qubits, diamond has been the material, very promising for optoelectronic and quantum device research [81]. Among more than 100 optically active defects in diamond, nitrogen vacancy (NV) center is the most interesting one due to its long coherence time, and bright red fluorescence with a zero phonon line (ZPL) at 637nm due to the optical transition between spin triplet states [82].

NV color center is a point defect in diamond, consisting of substitutional nitrogen-lattice vacancy pair oriented along the [111] crystalline direction [83]. The center exist in two charge states, which are the neutral NV^0 and the negatively charged NV^-. The identification of the NV^- and NV^0 centers is done using their characteristic ZPL emissions at 637 nm [84] and 575 nm [85]. The optical transition between the discrete vibronic states of the point defects result in sharp ZPLs.

A schematic of the NV center and diamond lattice depicting the vacancy (gray), the nearest neighbor carbon atoms to the vacancy (black), the substitutional nitrogen atom (blue), with the next-to-nearest carbon neighbors to the vacancy (black) is given in Fig. 5.1 (a). Fig. 5.1 (b) and (c) show the known features of the electronic structures of the NV^- and NV^0 with their optical ZPL emission energies. It should be noted that, the relative energies of the triplet (^3E, $^3A_2$) and singlet states ($^1A_1$, ^1E) of NV^- and the doublet (^2A, ^2E) and quartet states ($^4A_2$) of NV^0 are currently unknown [86].

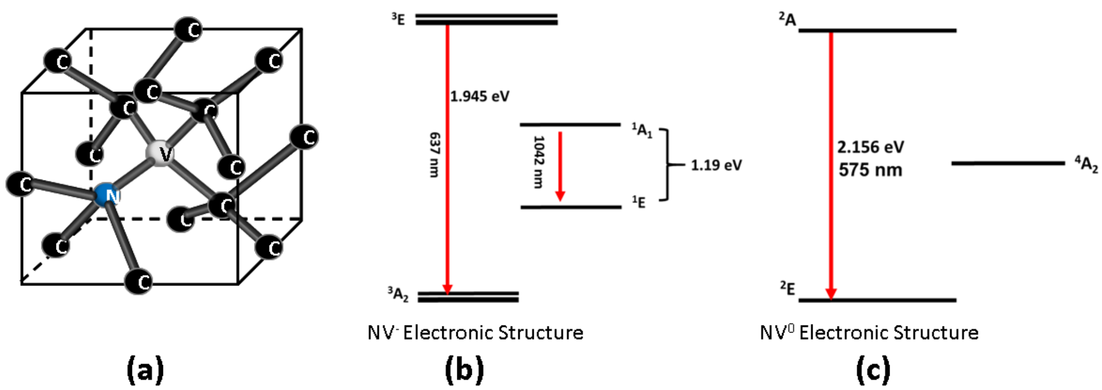

Fig. 5.1. (a) Schematic of the nitrogen-vacancy center and diamond lattice. (b) The known features of the electronic structure of the NV^- (c) The known features of the electronic structure of the NV^0.

5.2. Diamond Waveguides

The waveguide structures are fabricated on a commercially available (MB Optics) diamond bulk material (5 mm x 5 mm x 0.5 mm) using femtosecond laser inscription. The diamond sample is synthetically grown from a single crystal orientation, which is in optical grade, and polished to achieve smooth planar surface morphology. An amplified Yb:KGW femtosecond pulsed laser, which operates at the fundamental wavelength of 515 nm with a repetition rate of 500 kHz (Pharos, Light Conversion) with 230 fs pulse duration is used to fabricate the waveguides. Since the induced refractive index change is negative [31], type II waveguides are manufactures in diamond bulk material. In order to achieve low insertion losses and better beam profile for coupling to the WGMs of Si microsphere, waveguides with different parameters, i.e., at depths of 10-30 μm, with the laser power of 30-40mW, corresponding to pulse energies of 60-80 nJ, and with the spacing of 17-19 μm are written on the diamond sample with 0.5 mm/s scanning speed. The femtosecond laser pulses are focused by a 100x oil immersion objective with 1.25 numerical aperture (*NA*). The overhead microscope image of the diamond waveguides with thicknesses between d = 10-20 μm and widths between w = 17 – 19 μm are shown in Fig. 5.2. The power sets of the same thickness group are separated by 50 μm spacing, while the thickness groups are separated by 60 μm spacing.

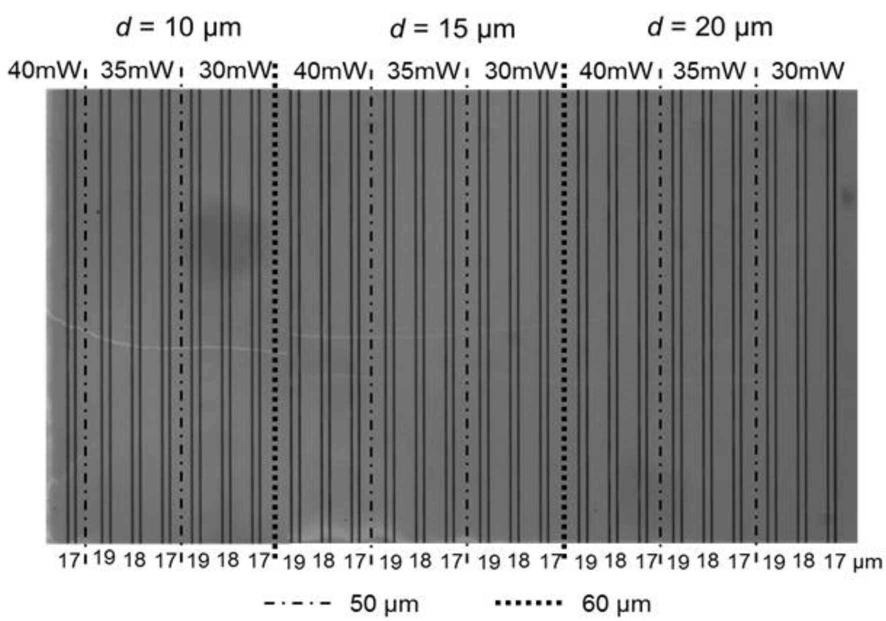

Fig. 5.2. Overhead microscope image of the waveguides written inside diamond.

The most promising waveguide, which is written with 30 mW laser power at a depth of 10 µm, and having a width of 19 µm is selected for Si microsphere WGM coupling. The insertion loss is measured as 12.43 dB by using butt-coupled, pigtailed single mode fiber (SMF) operating at 1550 nm. The mode field diameter (MDF) is measured as 16.4 µm x 20.5 µm in the horizontal and vertical directions, respectively. The near-field waveguide mode acquired by imaging the light using a beam profiler with a 60x aspheric lens, and the scanning electron microscopy (SEM) image of side view of the corresponding photo-inscribed WGs is shown in Fig. 5.3(a) and (b). The waveguide exhibit a single mode beam profile with an elliptical mode shape.

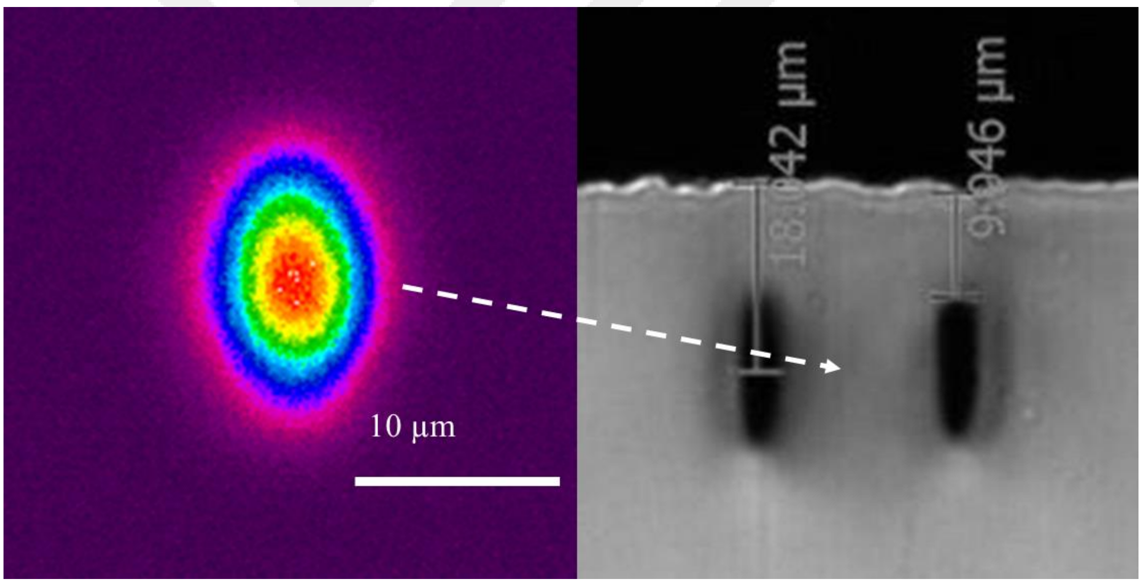

Fig. 5.3. (a) MFD profile (b) SEM image of the side view of the waveguide used for coupling for coupling to microsphere WGMs.

5.3. Experimental Setup

The experimental setup for coupling to Si microsphere WGMs using femtosecond laser inscribed diamond waveguides, and for measuring the elastic scattering and transmission intensities in the near-IR is shown in Fig. 5.4. The inset represent the side view of the bare fiber coupling to the diamond waveguide, and WGM coupling to the Si microsphere, where k denotes the wavevector.

The same DFB semiconductor diode laser, explained in Chapter 4 is used as the excitation source. The diamond WG, with a refractive index of 2.38 in the corresponding wavelength regime [87], is fixed on a three dimensional translational stage with a range of 20 mm and step size of 20 µm. A microscope is anchored on top of the WG perpendicular to the transmission direction for collecting the 90º elastically scattered light. A microscope objective with 10x magnification is used to collect the elastically scattered photons, which then splits into two by a beamsplitter (BS) to monitor the position of the Si sphere on the waveguide by a visible camera. A Glan polarizer (GP) is placed between the beamsplitter and the InGaAs photodetector (PD1) stationed on a 10x microscope eyepiece, to select between the TM and TE polarized 90º elastically scattered photons.

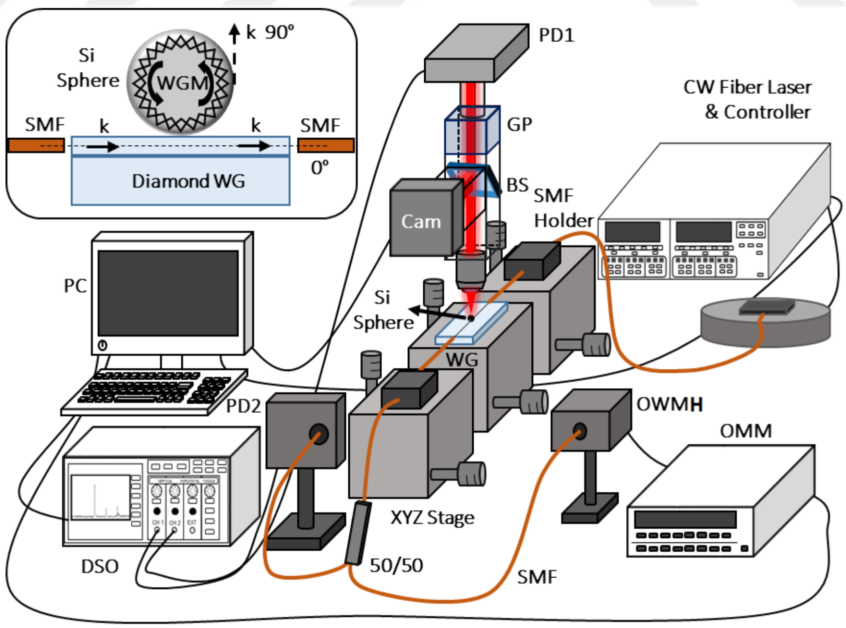

Fig. 5.4. The experimental setup for coupling to Si microsphere WGMs using femtosecond laser inscribed diamond waveguides, and for measuring the elastic scattering and transmission intensities.

The insertion of the light to the waveguide, and collection of the light from the waveguide is achieved using bare SMFs, which are placed on precision translational stages for their precise positioning with respect to the diamond waveguide. The visible image of the top view of the bare SMF butt coupling to the selected waveguide is shown in Fig. 5.5.

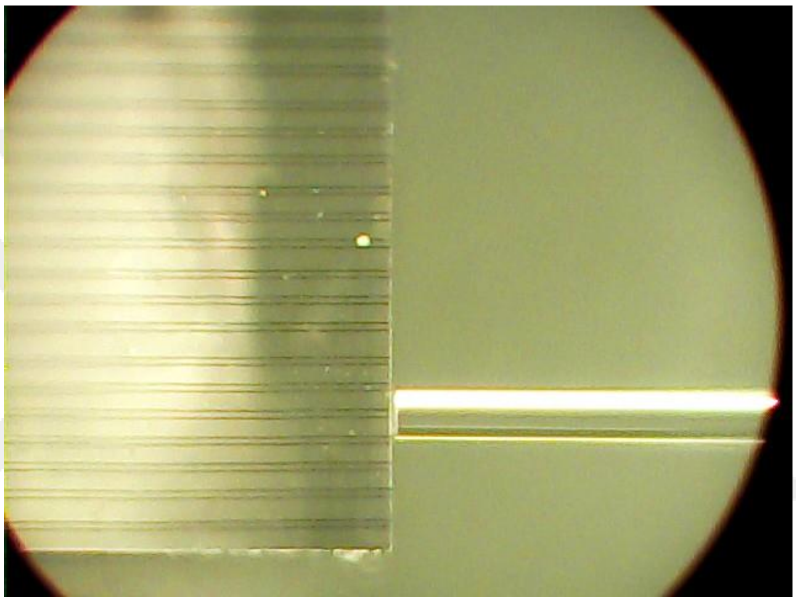

Fig. 5.5 Visible image (top view) of the femtosecond laser written waveguides on the diamond sample. 5th waveguide from bottom is butt coupled to a bare SMF.

The transmission is separated into two optical fibers by a 50/50 optical Y-coupler, where one channel is used to acquire the transmitted power by another InGaAs detector (PD2), while the other channel is connected to an optical wavemeter head (OWMH) controlled by an optical multimeter (OMM) to monitor the wavelength of the DFB laser. The outputs of the PD1 and PD2 are fed into a digital storage oscilloscope (DSO) to monitor 90º elastic scattering and 0º transmission, respectively. Data acquisition is performed by a standard IEEE-488 GPIB interface, along with LabView (National Instruments) software to construct the corresponding scattering and transmission spectra.

Positioning of the Si sphere (the same Si microsphere used in Chapter 4) is achieved in the same manner as described in Chapter 4. A vacuum pump attached to a thin needle tip is fixed to an additional XYZ micrometer stage is used to position the Si sphere on the WG platform to adjust the optimal coupling location. The needle tip holds the Si microsphere, which is brought to the close proximity of the photowritten waveguide on the diamond platform. The visible image of the Si spherical microresonator gripped by the suction mechanism on top of the diamond WG platform is shown in Fig. 5.6.

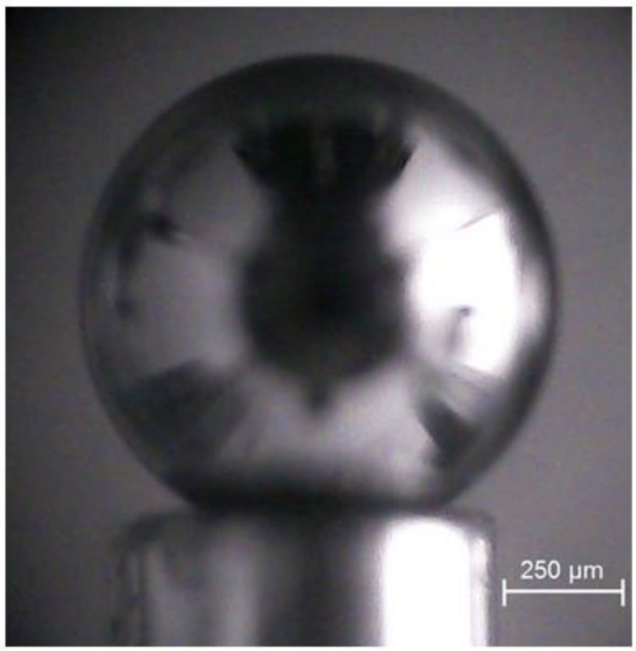

Fig. 5.6 Visible image (top view) of the Si microsphere held by the needle at the tip of the suction mechanism for positioning on top of the diamond waveguide platform.

5.4. Experimental Results

Fig. 5.7 shows the measured (a) 90° TM and (b) TE polarized elastic scattering and the 0° spectra. The calculated mode spacing of WGMs at the resonance wavelength is found as $\Delta\lambda$ = 0.249 nm. The TM (TE) polarized 90° elastic scattering is measured by placing the

GP in parallel (perpendicular) direction to the transmission direction of the guiding line on diamond platform. The measured mode spacing is $\Delta\lambda$ = 0.257 nm, corresponding to the spacing between the consecutive mode families with decreasing polar mode number, which are located at 1426.42 nm, 1426.67 nm, and 1426.94 nm. Similar to the TM polarization, a mode spacing of 0.257 nm is observed from TE polarized elastically scattered WGMs spectra with resonant wavelengths located at 1426.72 nm, 1426.98 nm, 1427.25 nm and 1427.53 nm. The calculated value and measured mode spacing at both polarizations are thus consistent with each other.

The oscillation in the both transmission spectra exhibits a periodicity of 0.087 nm. This periodicity corresponds to mode spacing of a Fabry-Pérot resonator [88] made of diamond with a cavity length of 5 mm; and is most probably caused by the back reflected waves at both ends of the diamond waveguide, which are butt coupled to optical bare fibers.

The maximum measured Q-factor is 6.2 x 10^4, which is centered at 1427.34 nm with a FWHM of 23 pm for 90º TM polarized elastic scattering. The maximum measurable Q-factor is limited by the resolution of the measurement setup, which is determined by the step size of the fine-tuned laser and is 1 pm. Despite a minor difference, the measured TE and TM polarized quality factors are comparable with each other.

The obtained results manifest coupling to silicon microsphere WGMs from the fs-laser written diamond waveguides, yielding high Q-factors due to the long lifetime of the photons circumnavigating the silicon microsphere.

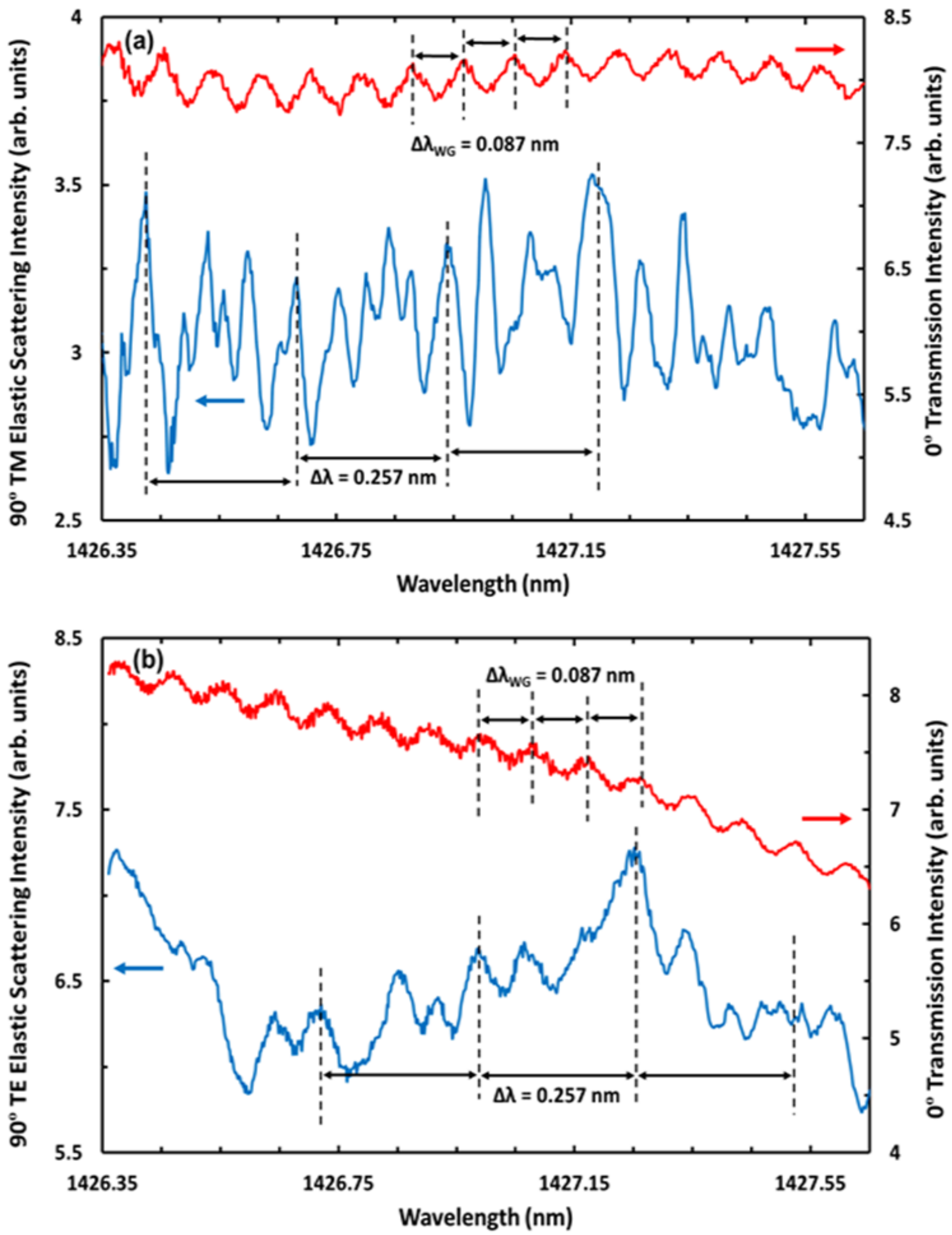

Fig. 5.7. (a) TM and (b) TE polarized elastically scattering spectrum at 90° (blue lower curve), and their corresponding transmission spectrum at 0° (red upper curve)

Chapter 6

EXCITATION OF DIAMOND SPHERE WGMS WITH GLASS OPTICAL FIBER HALF COUPLER

In addition to its unique color centers explained in Chapter 5.1, diamond exhibits further distinctive optical properties such as broad transmission range from ultraviolet (UV) to far-infrared (far-IR), wide electronic bandgap (5.5 eV), and large Raman gain [89]. Furthermore, its unique lattice structure, robust physical properties such as high thermal conductivity, high density, and high ignition point made diamond the material of interest for applications in electronics [90], quantum information processing [91], and sensing [92]. These applications can be further improved by introducing high Q-factor diamond microsphere resonators.

In this chapter, excitation results of WGM resonances of a synthetic diamond microsphere having a radius of 500 µm, using a silica optical fiber half coupler (OFHC) is presented. A distributed feedback (DFB) diode laser operating in the near-infrared (near-IR) is input to the OFHC. The WGM spectra exhibit Q-factors on the order of 10^4.

6.1. Experimental Setup

Fig. 6.1 shows the experimental setup used to excite the diamond microsphere WGMs using a glass OFHC for the measurement of 90° elastic scattering and 0° transmission spectra. The OFHC, which is anchored on top of a three-dimensional translational stage with a range of 20 mm and resolution of 20 µm, is connected to the pigtailed DFB diode laser, whereas the output of OFHC is connected to an InGaAs photodetector (PD1) to acquire the transmission spectrum.

Another InGaAs photodetector (PD2) is used along with a microscope, having a 20x magnification-objective, to collect the photons, which are elastically scattered perpendicular to the transmission direction. A Glan polarizer (GP) is used before PD2 in order to select between TE and TM polarizations of the elastically scattered light. The position of the microsphere, relative to the OFHC is monitored by a visible camera, by the help of a beamsplitter (BS) inside the microscope.

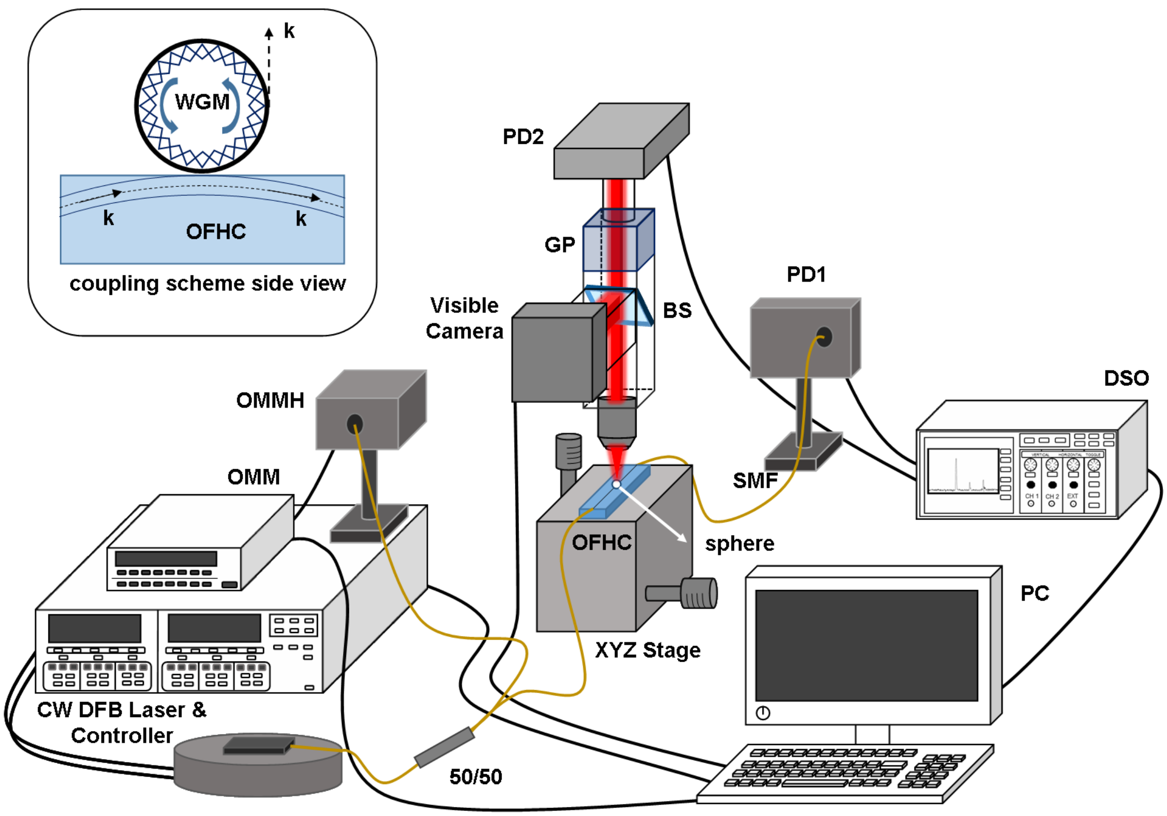

Fig. 6.1. Experimental setup used for the excitation of diamond microsphere WGMs using an OFHC and the measurement of 90° scattering and 0° transmission spectra

DFB diode laser output wavelength control between 1426.10 nm and 1427.42 nm, with a spectral resolution of 1 pm, is achieved by fine tuning the laser temperature. The output optical power of the laser is monitored by an optical multimeter head (OMMH) connected to an optical multimeter (OMM).

A control PC is connected to the laser diode controller (LDC), the optical multimeter, the visible camera, and the digital storage oscilloscope, which is used to acquire signals from PD1 and PD2. The automation and the data acquisition are done using LabView (National Instruments) software.

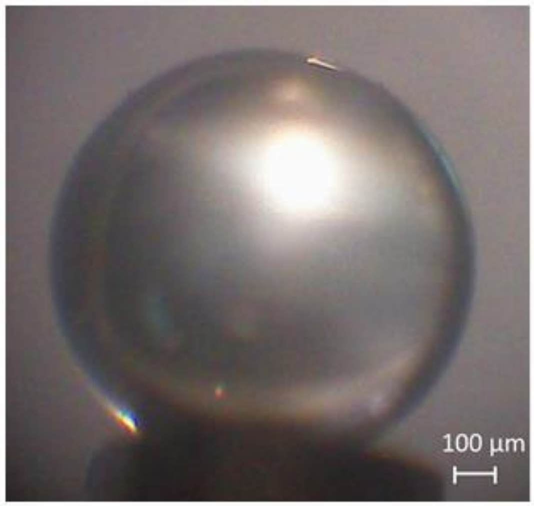

Fig. 6.2. Image of the diamond microsphere acquired using a visible camera

The inset of Fig. 6.1 shows the side view of the coupling scheme of the diamond microsphere with the OFHC, where k denotes the wavevector. The diamond sphere is held with the same technique with Chapters 4 and 5, using a thin needle tip connected to a vacuum suction tube. Fig. 6.2 illustrates an image of the diamond sphere (top view), held by the thin needle. The diamond sphere is synthetically grown by chemical vapor deposition (CVD). A monocrystalline diamond sphere was manufactured with 500 μm radius. Spherical geometry of the diamond is achieved by a specialized lapping machinery with a roundness defined by its form accuracy < 250 nm. The surface of the sample is polished to minimize the surface roughness, and to realize the required smooth surface finish for the WGMs. The refractive index of diamond in the near-IR is 2.38 [87], providing the required index difference to confine the photons around the sphere.

6.2. Experimental Results

Fig. 6.3 (a) shows the TM polarized and Fig. 6.3 (b) shows the TE polarized 90° scattering (blue curves) spectra of the WGM resonances obtained from the diamond sphere, where their respective 0° transmission spectra are shown with red curves. TM polarization of the elastically scattered light is acquired by placing the GP parallel to the transmission direction. Four resonant peaks located at 1426.29 nm, 1426.63 nm, 1426.96 nm, and 1427.28 nm denote the consecutive mode families with decreasing mode numbers are indicated with the dashed lines in Fig. 6.3(a). However, the corresponding resonance dips are not observable in the transmission spectrum at the resonance wavelengths. The mode spacing $\Delta\lambda$ is calculated as 0.340 nm for the diamond microsphere at 1426 nm, which is comparable to the experimentally measured value of 0.332 nm. The TE polarized elastically scattered light is acquired by placing the GP perpendicular to the transmission direction. The resulting spectrum in Fig. 6.3(b) exhibits the mode spacing of $\Delta\lambda = 0.332$ nm, which is identical with the mode spacing value for the TM polarization. The maximum Q-factor is calculated as 5.1 x 10^4, with $\delta\lambda = 28$ pm at the central resonant wavelength of 1426.80 nm of the TE polarized 90° elastic scattering spectra.

For our diamond sphere with $2a/\lambda > 15$, the intrinsic radiative losses contributing to Q_{rad} [93], and the loss caused by the surface contaminants contributing to Q_{cont} [58] can be neglected. The estimated Q_{ss} is on the order of 10^8, using (2.26) where σ and B are estimated to be 20 nm on the surface. Q_{mat} is estimated to be on the order of 10^5 ,where the refractive index of the diamond is 2.38, and the attenuation coefficient $\alpha < 1$ cm^{-1}, depending on the nitrogen concentration inside the diamond lattice [94]. For our case of undercoupling to the microsphere, Q_{ext} is negligible since Q-factors of 10^8 is achievable depending on the value of $|t|$.

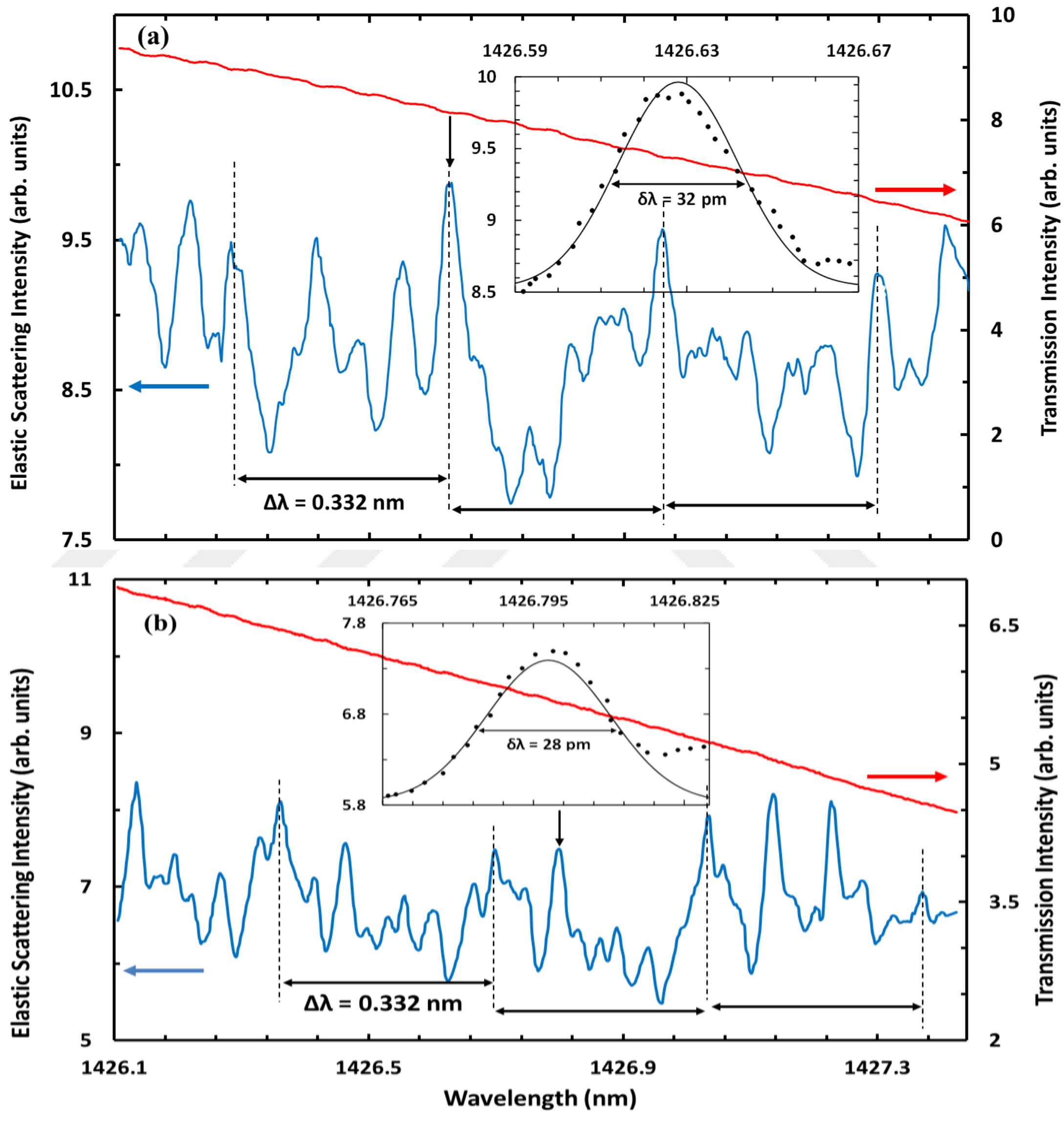

Fig. 6.3. (a) TM polarized (b) TE polarized 90º elastic scattering and 0º transmission spectra from diamond sphere WGMs. The FWHM of the resonances are calculated by Lorentz shape fitting the WGM peak as shown in the insets.

Chapter 7

CONCLUSIONS AND FUTURE WORK

Light coupling to microsphere whispering gallery modes (WGMs) of silicon microspheres is successfully realized using femtosecond laser micromachined glass and diamond waveguides. Observed high quality factors are comparable with each other and around 10^5. Femtosecond laser inscription is shown to be an alternative method for evanescent wave coupling to microsphere WGMs, providing a compact and robust platform for further applications.

In addition to utilizing diamond as waveguide material, WGMs of a diamond microsphere is excited using an optical fiber half coupler (OFHC). Employment of diamond material as a excitation platform or a high-Q cavity can lead to further applications exploiting the combination of WGM properties such as extreme mode confinement in small volumes, high power density, and long photon lifetime inside a cavity; with the unique optical properties of diamond such as existence of various color centers, broad transmission range from ultraviolet to far-infrared, wide electronic bandgap, and large Raman gain.

The performed experiments can be further improved with a stable and precise control of the excitation geometry and the impact parameter, i.e., position of the microsphere relative to the excitation beam. This stable and precise control of excitation geometry can enhance the evanescent wave coupling efficiency of the excitation beam to the microsphere WGMs, leading to possible higher quality factors, and observance of resonance dips in transmission spectra.

Diamond has been employed as both the femtosecond laser inscribed waveguide and the microsphere material, proving its suitability for both applications. Using diamond both as an excitation platform and a cavity to support high-Q WGMs in future experiments can lead to all-diamond photonic circuits.

VITA

Hüseyin Ozan Çirkinoğlu completed his high school education in İzmir Bornova Anadolu Lisesi in 2010.

He received his Bachelor of Science degree in Electronics and Communication Engineering from Istanbul Technical University, Turkey in 2015. He worked on "MEMS Based Fiber Optic Coupled Temperature Sensor" as his undergraduate thesis with Assistant Professor Onur Ferhanoğlu at Istanbul Technical University Electro-Optic Devices Laboratory.

He then joined the Master of Science program in Optoelectronics and Photonics Engineering at Koç University in Istanbul, Turkey in 2015, as a teaching/research assistant during which, he worked on "Excitation of Silicon and Diamond Microsphere Whispering Gallery Modes by Femtosecond Laser Written Glass and Diamond Waveguides and a Glass Optical Fiber Half Coupler" with Professor Ali Serpengüzel at Koç University Microphotonics Research Laboratory.

BIBLIOGRAPHY

[1] Lord Rayleigh, "The problem of the whispering gallery," The London, Edinburgh, and Dublin Philosophical Magazine and Journal of Science **20**, 1001–1004 (1910).

[2] C. Raman, "On whispering galleries," Bulletin of the Indian Association for the Cultivation of Science **7**, 159-172 (1922).

[3] G. Righini, Y. Dumeige, P. Féron, M. Ferrari, G. Nunzi Conti, D. Ristic, and S. Soria, "Whispering gallery mode microresonators: fundamentals and applications," Rivista del Nuovo Cimento **34**, 435–488 (2011).

[4] R. Richtmyer, "Dielectric resonators," Journal of Applied Physics **10**, 391–398 (1939).

[5] C. Garrett, W. Kaiser, and W. Bond, "Stimulated emission into optical whispering modes of spheres," Physical Review **124**, 1807 (1961).

[6] A. Ashkin and J. Dziedzic, "Observation of resonances in the radiation pressure on dielectric spheres," Physical Review Letters **38**, 1351 (1977).

[7] R. Benner, P. Barber, J. Owen, and R. Chang, "Observation of structure resonances in the fluorescence spectra from microspheres," Physical Review Letters **44**, 475 (1980).

[8] T. J. Kippenberg, J. Kalkman, A. Polman, and K. J. Vahala, "Demonstration of an erbium-doped microdisk laser on a silicon chip," Physical Review A **74**, 051802 (2006).

[9] S. Chang, N. B. Rex, R. K. Chang, G. Chong, and L. J. Guido, "Stimulated emission and lasing in whispering-gallery modes of GaN microdisk cavities," Applied Physics Letters **75**, 166–168 (1999).

[10] L. Feng, Z. J. Wong, R.-M. Ma, Y. Wang, and X. Zhang, "Single-mode laser by parity-time symmetry breaking," Science **346**, 972–975 (2014).

[11] H.-Y. Ryu, S.-H. Kim, H.-G. Park, J.-K. Hwang, Y.-H. Lee, and J.-S. Kim, "Square-lattice photonic band-gap single-cell laser operating in the lowest-order whispering gallery mode," Applied Physics Letters **80**, 3883–3885 (2002).

[12] F. Albert, T. Braun, T. Heindel, C. Schneider, S. Reitzenstein, S. Höfling, L. Worschech, and A. Forchel, "Whispering gallery mode lasing in electrically driven quantum dot micropillars," Applied Physics Letters **97**, 101108 (2010).

[13] V. Astratov, S. Yang, S. Lam, B. Jones, D. Sanvitto, D. Whittaker, A. Fox, M. Skolnick, A. Tahraoui, and P. Fry, "Whispering gallery resonances in semiconductor micropillars," Applied Physics Letters **91**, 071115 (2007).

[14] T. Kippenberg, S. Spillane, D. Armani, and K. Vahala, "Ultralow-threshold microcavity Raman laser on a microelectronic chip," Optics Letters **29**, 1224–1226 (2004).

[15] M. Cai, G. Hunziker, and K. Vahala, "Fiber-optic add-drop device based on a silica microsphere-whispering gallery mode system," IEEE Photonics Technology Letters **11**, 686–687 (1999).

[16] A. Chiasera, Y. Dumeige, P. Féron, M. Ferrari, Y. Jestin, G. Nunzi Conti, S. Pelli, S. Soria, and G. C. Righini, "Spherical whispering-gallery-mode microresonators," Laser & Photonics Reviews **4**, 457–482 (2010).

[17] M. Noto, D. Keng, I. Teraoka, and S. Arnold, "Detection of protein orientation on the silica microsphere surface using transverse electric/transverse magnetic whispering gallery modes," Biophysical Journal **92**, 4466–4472 (2007).

[18] A. Serpengüzel, Y. O. Yılmaz, U. K. Ayaz, and A. Kurt, "Silicon Microspheres for VLSI Photonics," in *VLSI Micro- and Nanophotonics: Science, Technology, and Applications* (CRC Press, Boca Raton, Florida 2011).

[19] V. S. Ilchenko, A. A. Savchenkov, A. B. Matsko, and L. Maleki, "Whispering-gallery-mode electro-optic modulator and photonic microwave receiver," Journal of the Optical Society of America B **20**, 333–342 (2003).

[20] C. Wang, Y. Choi, J. Lee, E. Hu, J. Yang, and J. Butler, "Observation of whispering gallery modes in nanocrystalline diamond microdisks," Applied Physics Letters **90**, 081110 (2007).

[21] H.-M. Tzeng, K. F. Wall, M. Long, and R. Chang, "Laser emission from individual droplets at wavelengths corresponding to morphology-dependent resonances," Optics Letters **9**, 499–501 (1984).

[22] V. Sandoghdar, F. Treussart, J. Hare, V. Lefèvre-Seguin, J.-M. Raimond, and S. Haroche, "Very low threshold whispering-gallery-mode microsphere laser," Physical Review A **54**, R1777 (1996).

[23] A. A. Savchenkov, A. B. Matsko, V. S. Ilchenko, I. Solomatine, D. Seidel, and L. Maleki, "Tunable optical frequency comb with a crystalline whispering gallery mode resonator," Physical Review Letters **101**, 093902 (2008).

[24] Y. O. Yılmaz, A. Demir, A. Kurt, and A. Serpengüzel, "Optical channel dropping with a silicon microsphere," IEEE Photonics Technology Letters **17**, 1662–1664 (2005).

[25] V. S. Ilchenko, A. B. Matsko, A. A. Savchenkov, and L. Maleki, "Low-threshold parametric nonlinear optics with quasi-phase-matched whispering-gallery modes," Journal of the Optical Society of America B **20**, 1304–1308 (2003).

[26] S. Spillane, T. Kippenberg, and K. Vahala, "Ultralow-threshold Raman laser using a spherical dielectric microcavity," Nature **415**, 621–623 (2002).

[27] I. S. Grudinin, A. B. Matsko, and L. Maleki, "Brillouin lasing with a CaF 2 whispering gallery mode resonator," Physical Review Letters **102**, 043902 (2009).

[28] R. R. Gattass and E. Mazur, "Femtosecond laser micromachining in transparent materials," Nature Photonics **2**, 219–225 (2008).

[29] K. M. Davis, K. Miura, N. Sugimoto, and K. Hirao, "Writing waveguides in glass with a femtosecond laser," Optics Letters **21**, 1729–1731 (1996).

[30] K. Miura, J. Qiu, H. Inouye, T. Mitsuyu, and K. Hirao, "Photowritten optical waveguides in various glasses with ultrashort pulse laser," Applied Physics Letters **71**, 3329–3331 (1997).

[31] B. Sotillo, V. Bharadwaj, J. Hadden, M. Sakakura, A. Chiappini, T. T. Fernandez, S. Longhi, O. Jedrkiewicz, Y. Shimotsuma, and L. Criante, "Diamond photonics platform enabled by femtosecond laser writing," Nature Scientific Reports **6**, pages (2016).

[32] D. Parthenopoulos and P. Rentzepis, "Two-photon volume information storage in doped polymer systems," Journal of Applied Physics **68**, 5814–5818 (1990).

[33] C. B. Schaffer, A. Brodeur, J. F. García, and E. Mazur, "Micromachining bulk glass by use of femtosecond laser pulses with nanojoule energy," Optics Letters **26**, 93–95 (2001).

[34] H.-B. Sun, Y. Xu, S. Juodkazis, K. Sun, M. Watanabe, S. Matsuo, H. Misawa, and J. Nishii, "Arbitrary-lattice photonic crystals created by multiphoton microfabrication," Optics Letters **26**, 325–327 (2001).

[35] R. Osellame, V. Maselli, R. M. Vazquez, R. Ramponi, and G. Cerullo, "Integration of optical waveguides and microfluidic channels both fabricated by femtosecond laser irradiation," Applied Physics Letters **90**, 231118 (2007).

[36] G. Della Valle, R. Osellame, and P. Laporta, "Micromachining of photonic devices by femtosecond laser pulses," Journal of Optics A: Pure and Applied Optics **11**, 013001 (2008).

[37] M. Gorodetsky and V. Ilchenko, "High-Q optical whispering-gallery microresonators: precession approach for spherical mode analysis and emission patterns with prism couplers," Optics Communications **113**, 133–143 (1994).

[38] V. S. Ilchenko, X. S. Yao, and L. Maleki, "Pigtailing the high-Q microsphere cavity: a simple fiber coupler for optical whispering-gallery modes," Optics Letters **24**, 723–725 (1999).

[39] A. Serpengüzel, G. Griffel, and S. Arnold, "Excitation of resonances of microspheres on an optical fiber," Optics Letters **20**, 654–656 (1995).

[40] Y. Panitchob, G. S. Murugan, M. Zervas, P. Horak, S. Berneschi, S. Pelli, G. N. Conti, and J. Wilkinson, "Whispering gallery mode spectra of channel waveguide coupled microspheres," Optics Express **16**, 11066–11076 (2008).

[41] D. H. Broaddus, M. A. Foster, I. H. Agha, J. T. Robinson, M. Lipson, and A. L. Gaeta, "Silicon-waveguide-coupled high-Q chalcogenide microspheres," Optics Express **17**, 5998–6003 (2009).

[42] P. Debye, "Der lichtdruck auf kugeln von beliebigem material," Annalen der Physik **335**, 57–136 (1909).

[43] A. N. Oraevsky, "Whispering-gallery waves," Quantum Electronics **32**, 377–400 (2002).

[44] M. J. Humphrey, "Calculation of coupling between tapered fiber modes and whispering-gallery modes of a spherical microlaser," Oklahoma State University (2004).

[45] P. Chýlek, "Partial-wave resonances and the ripple structure in the Mie normalized extinction cross section," Journal of the Optical Society of America **66**, 285–287 (1976).

[46] S. Schiller and R. L. Byer, "High-resolution spectroscopy of whispering gallery modes in large dielectric spheres," Optics Letters **16**, 1138–1140 (1991).

[47] H. Lai, P. Leung, K. Young, P. Barber, and S. Hill, "Time-independent perturbation for leaking electromagnetic modes in open systems with application to resonances in microdroplets," Physical Review A **41**, 5187 (1990).

[48] T. Bilici, Ş. İşçi, A. Kurt, and A. Serpengüzel, "GaInNAs microspheres for wavelength division multiplexing," IEE Proceedings - Optoelectronics **150**, 89–91 (2003).

[49] H. Mabuchi and H. Kimble, "Atom galleries for whispering atoms: binding atoms in stable orbits around an optical resonator," Optics Letters **19**, 749–751 (1994).

[50] M. L. Gorodetsky, A. A. Savchenkov, and V. S. Ilchenko, "Ultimate Q of optical microsphere resonators," Optics Letters **21**, 453–455 (1996).

[51] G. Griffel, J. Connolly, N. Morris, S. Arnold, D. Taşkent, and A. Serpengüzel, "Morphology-dependent resonances of a microsphere–optical fiber system," Optics Letters **21**, 695–697 (1996).

[52] M. Cai and K. Vahala, "Highly efficient hybrid fiber taper coupled microsphere laser," Optics Letters **26**, 884–886 (2001).

[53] V. Braginsky, M. Gorodetsky, and V. Ilchenko, "Quality-factor and nonlinear properties of optical whispering-gallery modes," Physics Letters A **137**, 393–397 (1989).

[54] G. Cerullo, R. Osellame, S. Taccheo, M. Marangoni, D. Polli, R. Ramponi, P. Laporta, and S. De Silvestri, "Femtosecond micromachining of symmetric waveguides at 1.5 μm by astigmatic beam focusing," Optics Letters **27**, 1938–1940 (2002).

[55] B. E. Little, J.-P. Laine, and H. A. Haus, "Analytic theory of coupling from tapered fibers and half-blocks into microsphere resonators," Journal of Lightwave Technology **17**, 704 (1999).

[56] H. Van de Hulst, "Light Scattering by Small Particles," Dover, New York, 208 (1981).

[57] J. A. Lock, "Improved Gaussian beam-scattering algorithm," Applied Optics **34**, 559–570 (1995).

[58] A. Serpengüzel, S. Arnold, G. Griffel, and J. A. Lock, "Enhanced coupling to microsphere resonances with optical fibers," Journal of the Optical Society of America B **14**, 790–795 (1997).

[59] K. D. Webb, M. S. Murib, A. Serpengüzel, and R. Beccherelli, "Electrooptical tuning of a ruby microsphere morphology dependent resonance in a liquid crystal medium," in Proceedings of the IEEE Photonics Technology Society Annual Meeting, pp. 328–329 (2009).

[60] N. Bloembergen, "A brief history of light breakdown," Journal of Nonlinear Optical Physics & Materials **6**, 377–385 (1997).

[61] R. Osellame, G. Cerullo, and R. Ramponi, *Femtosecond Laser Micromachining: Photonic and Microfluidic Devices in Transparent Materials* (Springer Science & Business Media, 2012), Vol. 123.

[62] Y. Peng, Y. Wei, and Z. Lv "Femtosecond laser-induced damage in dielectrics," Optica Applicata **34**, 319–330 (2004).

[63] M. Ams, G. D. Marshall, P. Dekker, M. Dubov, V. K. Mezentsev, I. Bennion, and M. J. Withford, "Investigation of Ultrafast Laser--Photonic Material Interactions: Challenges for Directly Written Glass Photonics," IEEE Journal of Selected Topics in Quantum Electronics **14**, 1370–1381 (2008).

[64] C. B. Schaffer, A. Brodeur, and E. Mazur, "Laser-induced breakdown and damage in bulk transparent materials induced by tightly focused femtosecond laser pulses," Measurement Science and Technology **12**, 1784 (2001).

[65] L. V. Keldysh, "Ionization in the field of a strong electromagnetic wave," Sov. Phys. Journal of Experimental Theoretical Physics **20**, 1307–1314 (1965).

[66] R. Mary, D. Choudhury, and A. K. Kar, "Applications of fiber lasers for the development of compact photonic devices," IEEE Journal of Selected Topics in Quantum Electronics **20**, 72–84 (2014).

[67] B. C. Stuart, M. D. Feit, S. Herman, A. Rubenchik, B. Shore, and M. Perry, "Nanosecond-to-femtosecond laser-induced breakdown in dielectrics," Physical Review B **53**, 1749 (1996).

[68] J. Chan, T. Huser, S. Risbud, and D. Krol, "Structural changes in fused silica after exposure to focused femtosecond laser pulses," Optics letters **26**, 1726–1728 (2001).

[69] A. M. Streltsov and N. F. Borrelli, "Study of femtosecond-laser-written waveguides in glasses," Journal of the Optical Society of America B **19**, 2496–2504 (2002).

[70] B. Poumellec and M. Lancry, "Damage thresholds in femtosecond laser processing of silica based materials," in (Sydney, NSW, Australia, 2006), pp. 91–105.

[71] Y. Shimotsuma, P. G. Kazansky, J. Qiu, and K. Hirao, "Self-organized nanogratings in glass irradiated by ultrashort light pulses," Physical Review Letters **91**, 247405 (2003).

[72] L. Sudrie, M. Franco, B. Prade, and A. Mysyrowicz, "Writing of permanent birefringent microlayers in bulk fused silica with femtosecond laser pulses," Optics Communications **171**, 279–284 (1999).

[73] E. N. Glezer and E. Mazur, "Ultrafast-laser driven micro-explosions in transparent materials," Applied Physics Letters **71**, 882–884 (1997).

[74] K. Itoh, W. Watanabe, S. Nolte, and C. B. Schaffer, "Ultrafast processes for bulk modification of transparent materials," Materials Research Society bulletin **31**, 620–625 (2006).

[75] C. Mendez, J. V. de Aldana, G. Torchia, and L. Roso, "Optical waveguide arrays induced in fused silica by void-like defects using femtosecond laser pulses," Applied Physics B **86**, 343–346 (2007).

[76] W. Watanabe, T. Toma, K. Yamada, J. Nishii, K. Hayashi, and K. Itoh, "Optical seizing and merging of voids in silica glass with infrared femtosecond laser pulses," Optics Letters **25**, 1669–1671 (2000).

[77] N. Takeda, "Spherical silicon 1 mm device and its clustering," in Proceedings of International Symposium on Advanced Packaging Materials: Processes, Properties and Interfaces (IEEE) 86–91. (2001)

[78] P. J. Mohr, D. B. Newell, and B. N. Taylor, "CODATA recommended values of the fundamental physical constants: 2014," Journal of Physical and Chemical Reference Data **45**, 043102 (2016).

[79] M. S. Murib, E. Yüce, O. Gürlü, and A. Serpengüzel, "Polarization behavior of elastic scattering from a silicon microsphere coupled to an optical fiber," Photonics Research **2**, 45–50 (2014).

[80] I. Aharonovich, A. D. Greentree, and S. Prawer, "Diamond photonics," Nature Photonics **5**, 397–405 (2011).

[81] J. Wrachtrup and F. Jelezko, "Processing quantum information in diamond," Journal of Physics: Condensed Matter **18**, S807 (2006).

[82] D. D. Awschalom, R. Epstein, and R. Hanson, "Spintronics," Scientific American (2007).

[83] G. Davies and M. Hamer, "Optical studies of the 1.945 eV vibronic band in diamond," in Proceedings of the Royal Society A: Mathematical, Physical and Engineering Sciences, **348**, 285–298 (1976).

[84] H. Dyer, F. Raal, L. Du Preez, and J. Loubser, "Optical absorption features associated with paramagnetic nitrogen in diamond," Philosophical Magazine **11**, 763–774 (1965).

[85] G. Davies, "Dynamic Jahn-Teller distortions at trigonal optical centres in diamond," Journal of Physics C: Solid State Physics **12**, 2551 (1979).

[86] M. W. Doherty, N. B. Manson, P. Delaney, F. Jelezko, J. Wrachtrup, and L. C. Hollenberg, "The nitrogen-vacancy colour centre in diamond," Physics Reports **528**, 1–45 (2013).

[87] H. Phillip and E. Taft, "Kramers-Kronig analysis of reflectance data for diamond," Physical Review **136**, A1445 (1964).

[88] C. J. Hood, H. Kimble, and J. Ye, "Characterization of high-finesse mirrors: Loss, phase shifts, and mode structure in an optical cavity," Physical Review A **64**, 033804 (2001).

[89] J. Walker, "Optical absorption and luminescence in diamond," Reports on Progress in Physics **42**, 1605 (1979).

[90] E. Kohn and A. Denisenko, "Concepts for diamond electronics," Thin Solid Films **515**, 4333–4339 (2007).

[91] S. Prawer and I. Aharonovich, *Quantum Information Processing with Diamond: Principles and Applications* (Elsevier, 2014).

[92] I. Teraoka, S. Arnold, and F. Vollmer, "Perturbation approach to resonance shifts of whispering-gallery modes in a dielectric microsphere as a probe of a surrounding medium," Journal of Optical Society of America B **20**, 1937–1946 (2003).

[93] V. Ilchenko, M. Gorodetsky, and S. Vyatchanin, "Coupling and tunability of optical whispering-gallery modes: a basis for coordinate meter," Optics Communications **107**, 41–48 (1994).

[94] R. U. A. Khan, P. M. Martineau, B. Cann, M. Newton, and D. Twitchen, "Charge transfer effects, thermo and photochromism in single crystal CVD synthetic diamond," Journal of Physics: Condensed Matter **21**, 364214 (2009).